

## A novel approach for extracting functional brain networks involved in mesial temporal lobe epilepsy based on self organizing maps

Alireza Fallahi<sup>a,b,c</sup>, Mohammad Pooyan<sup>b</sup>, Jafar Mehvari Habibabadi<sup>d</sup>,  
Seyed Sohrab Hashemi-Fesharaki<sup>e</sup>, Narges Hoseini Tabatabaei<sup>f</sup>, Mohammadreza Ay<sup>c,g</sup>,  
Mohammad-Reza Nazem-Zadeh<sup>c,g,\*</sup>

<sup>a</sup> Biomedical Engineering, Hamedan University of Technology, Hamedan, Iran

<sup>b</sup> Biomedical Engineering Department, Shahed University, Tehran, Iran

<sup>c</sup> Research Center for Molecular and Cellular Imaging, Advanced Medical Technologies and Instruments Institute (AMTII), Tehran University of Medical Sciences, Tehran, Iran

<sup>d</sup> Isfahan Neuroscience Research Center, Isfahan University of Medical Sciences, Isfahan, Iran

<sup>e</sup> Pars Advanced Medical Research Center, Pars Hospital, Tehran, Iran

<sup>f</sup> Medical School, Tehran University of Medical Sciences, Tehran, Iran

<sup>g</sup> Physics and Biomedical Engineering Department, Tehran University of Medical Sciences, Tehran, Iran

### ARTICLE INFO

#### Keywords:

Functional brain networks  
Self-organizing maps  
Restricted frechet mean  
Mesial temporal lobe epilepsy

### ABSTRACT

**Purpose:** We propose a novel data-driven approach to extract and present large-scale functional brain networks from functional magnetic resonance imaging (fMRI) data using spatiotemporal self-organizing maps (STSOM) clustering, accounting for the properties of the brain functional networks being spatially structured and inter-hemispherically symmetric. Also, a novel group-wise analysis is proposed based on restricted Frechet mean to identify group-level networks. The alteration of resulted networks in left and right mesial temporal lobe epilepsy (mTLE) is studied.

**Methods:** Thirty-five unilateral mTLE patients (21 left-mTLE (LTLE) and 14 right-mTLE (RTLE)), were prospectively studied. Eleven healthy control (HC) subjects were also recruited. To determine the functional networks of the whole brain, we extracted individual and group-level networks using spatiotemporal self-organizing maps and the restricted Frechet mean method, respectively. We applied the resulted networks to specify within and between-network alteration in functional connectivity (FC) in the LTLE and RTLE patients compared to the control cohort.

**Results:** We obtained seven networks namely default-mode (DMN), sensorimotor (SMN), visual (VSN), subcortical (SCN), frontoparietal (FPN), dorsal attention (DAN), and ventral attention (VAN) networks. Our results demonstrated increased functional connectivity in the FPN networks in the LTLE and the RTLE cohorts compared to HC. Increased FC has been observed between DMN, FPN, DAN, VAN, and VSN in the LTLE cohort and between the DMN and FPN networks in the RTLE cohort.

**Conclusion:** The proposed method has obtained promising results within a range of SNR and properly overlapped with the well-known functional networks using the Hausdorff distance. The consistent alteration patterns in within-and between-network FC for LTLE and RTLE patient cohorts would reflect the reliability of identification of large-scale brain networks in patients with mTLE. Different pattern of alterations in LTLE and RTLE compare with HC groups may be useful for laterality purpose.

### 1. Introduction

Mesial temporal lobe epilepsy (mTLE) is the most common type of

drug-resistant focal epilepsy that involves the internal structures of the temporal lobe [1,2]. Recent research shows that mTLE not only affects the temporal lobe regions, but also manifests structural effects

\* Corresponding author. Research Center for Molecular and Cellular Imaging, Advanced Medical Technologies and Instruments Institute (AMTII), Tehran University of Medical Sciences, Tehran, Iran.

E-mail address: [mnazemzadeh@tums.ac.ir](mailto:mnazemzadeh@tums.ac.ir) (M.-R. Nazem-Zadeh).

<https://doi.org/10.1016/j.imu.2022.100876>

Received 11 December 2021; Received in revised form 4 February 2022; Accepted 5 February 2022

Available online 8 February 2022

2352-9148/© 2022 The Authors.

Published by Elsevier Ltd.

This is an open access article under the CC BY-NC-ND license

(<http://creativecommons.org/licenses/by-nc-nd/4.0/>).

extratemporally [3–5]. MRI volumetric analysis such as voxel-based morphometric (VBM) shows atrophy in the hippocampus as well as regions beyond the hippocampus within ipsilateral temporal lobe [6], thalamus [7–9], and cingulate cortex [10–12]. These structural abnormalities cause asymmetric features on the ipsilateral side to the epileptogenic zone [5,13,14]. Besides structural alterations, extensive and widespread functional and cognitive impairments by mTLE are evidenced by neuropsychological evaluations and neuroimaging approaches in temporal and extra-temporal brain networks known as resting-state network (RSN) and support the theory that mTLE is an extensive network disorder [15–18]. Different alterations by mTLE are reported including default mode (DMN), sensorimotor (SMN), subcortical (SCN), limbic (LIN), visual (VSN), frontoparietal (FPN), dorsal attention (DAN), and ventral attention (VAN) networks [17,19–21]. These networks involve various areas of the brain that are not necessarily spatially close, and exhibit an extremely similar pattern of blood oxygenation level-dependent (BOLD) signal identified by resting-state functional connectivity (RSFC) [22]. The BOLD signals from brain regions might be functionally correlated, yet are evidenced to be spatially structured reflecting the structural architecture and internally homogeneous and cytoarchitecturally organized structure of the cortical areas in the human brain [23–28]. In addition to the symmetrical pattern of the brain structures, previous research on RSFC demonstrates the symmetry of the brain functional networks for more than 95% in mean resting-state connectivity [29], and also equal distribution of ICA components in the two brain hemispheres [24,30,31]. Therefore, the symmetrical properties can be accounted for to identify brain functional networks. Considering the fact that the brain networks often function and structure interhemispherically symmetric in healthy brains and asymmetric in neurological diseases such as mTLE, we hypothesize that the use of spatial information along with the temporal correlations can better identify the brain networks and model and describe the alteration in mTLE [32,33].

Several methods have been applied to study functional networks utilizing resting-state fMRI (rsfMRI) data. Data-driven methods are among the most powerful and flexible approaches that can detect spatially and temporally correlated patterns without enforcing the observed data to fit into any specific model. Principal component analysis (PCA) [34,35], independent component analysis (ICA) [36,37], and data clustering methods [38–43] have been generally used as data-driven methods for fMRI analysis. The main clustering techniques are K-means [38,44], fuzzy clustering [39], hierarchical clustering [40]; and self-organizing maps (SOMs) [41–43]. Yet, each of these techniques has its own drawbacks. In the PCA technique, the components are assumed to be orthogonal, thus, only the second-order statistics (variance) are used. To describe the heterogeneously distributed fMRI dataset, the second-order statistics do not seem to be adequate and the assumption of orthogonality for the components may not be appropriate for fMRI data [45]. Using higher-order statistics (entropy-based or non-Gaussianity assumption), ICA may be able to separate independent components of the data. The strong assumption taken in this method is about the independence between spatial or temporal components which may lead to invalid decomposition [46,47]. In addition, no priority is designated to independent components and often they are difficult to interpret or assign to the effect of interest. The K-means clustering algorithm, on the other hand, constrains the clusters to be spherical and symmetrical, which confines its application in the real fMRI domain [38]. In the fuzzy clustering method, the limitation comes from the fact that the results strongly depend on assignment of initial cluster centers and the fuzzy factor [48]. The hierarchical clustering method eliminates some of the limitations of K-mean and fuzzy clustering algorithms, however, the inability to determine a specific threshold for integration or division, and perhaps the computational complexity are among their main disadvantages [38].

The SOM is an unsupervised neural network that provides nonlinear projection from a high-dimensional data on a 1D or 2D map, which is

shown to overcome the abovementioned limitations. The topology-preserving property of SOM reveals basic data structures [49,50] and has successfully been used in task fMRI as well as in rsfMRI data analysis [33,42].

Besides the choice of technique for extracting RSNs, another important decision to make is whether an individual- or a group-wise analysis has to be carried out. Even though the individual analysis may be useful for some purposes including individual-level precision, such analysis is limited by the quite low signal-to-noise ratio of fMRI and small effect size. Therefore, network analysis at the group level is more common, which is a complex task and, in some cases, requires human interference in the selection of algorithm parameters such as the number of networks to analyze.

In this paper, we took the properties of the brain being spatially structured and interhemispherical symmetric into account to extract functional RSNs using AAL atlas nodes. We proposed an integrated spatiotemporal clustering approach using self-organizing maps as a data-driven technique for identifying brain functional networks. Using a normal healthy group, we summarized individual cluster results to group representative networks. We constructed a group analysis approach for selecting consistently functionally connected RSNs using a restricted Frechet mean approach, that minimizes a sum of squared distances from all the elements in the defined space. In our framework these elements are represented with each SOM [51]. After performing the spatiotemporal SOM clustering method on individual subjects, we customized the restricted Frechet mean method to be used for group analysis of functional networks in normal subjects. We have validated our proposed method using a syntactically simulated data.

We used the obtained functional networks to investigate the functional connectivity abnormalities in patients with left and right mTLE (noted by LTLE and RTLE, respectively). To this end, we proposed and followed a three-step approach. In the first step, the functional networks in healthy individuals are estimated using the proposed spatiotemporal SOM clustering algorithm. In the second step, we used the SOM restricted Frechet mean method to identify group-wise functional networks. In the third step, using networks obtained from normal individuals, we examined the differences within and between-network connectivity in the functional networks for the mTLE patients.

## 2. Materials and methods

### 2.1. Subjects

This study included 35 unilateral mTLE patients (21 LTLE and 14 RTLE). The side of laterality was determined by team of neurologists, epileptologists, neuropsychologists, and the neurosurgeon in a multi-disciplinary presurgical decision-making session, based on descriptions and manifestation of seizure semiology, ictal EEG, ictal epileptogenic zone, and interictal-irritative zone, as well as MRI findings. The

**Table 1**  
Patient characteristic.

Characteristic	HC	LTLE	RTLE	P-Value		
				LTLE vs. RTLE	LTLE vs. HC	RTLE vs. HC
Sample size	11	21	14	–		
Sex (M/F)	5/6	10/11	8/6	0.73 <sup>a</sup>	1.00 <sup>a</sup>	0.69 <sup>a</sup>
Age (yr), mean ± STD	27.7 ± 4.2	31.9 ± 8.2	26.8 ± 6.2	0.06 <sup>b</sup>	0.12 <sup>b</sup>	0.72 <sup>b</sup>
[range]	[17–36]	[17–54]	[17–36]			
Onset Age (yr), mean ± STD	–	10.8 ± 8.2	9.4 ± 9.4	0.63 <sup>b</sup>	–	–
[range]		[0.5–28]	[0.5–28]			

<sup>a</sup> Fisher exact test.

<sup>b</sup> Two-sample *t*-test.

characteristic information of the patients is given in Table .1. Patients with disabling cognitive impairment or other patients with other neurological diseases were excluded beforehand. Eleven healthy subjects were also recruited as controls. All subjects in the control group were healthy and did not have any neurological or mental disorders at the time of the study. We asked all subjects to relax, close their eyes without sleeping, and think nothing in particular during MRI and fMRI scans. The research protocol was approved by the Institutional Review Board of Tehran University of Medical Sciences.

## 2.2. Image acquisition

MRI data were collected using a 64-channel phased-array head coil on a 3-T scanner (Siemens Prisma, Erlangen, Germany) with software version “Syngo MR E11” at the Iranian National Brain Mapping Laboratory (NMBL). Anatomic images were acquired for clinical diagnosis using a standard protocol including transverse T1 weighted images using MPRAGE protocol with the following imaging parameter: TR = 1840 ms, TI = 900 ms, TE = 2.43 ms, flip angle = 8°, matrix = 224 × 224, in-plane resolution = 1.0 × 1.0 mm<sup>2</sup>, slice thickness = 1.0 mm, pixel bandwidth = 250 Hz/pixel. The rsfMRI images were acquired using echo-planar imaging (EPI) protocol with 330 measurements and the imaging parameters: TR = 3000 ms, TE = 30 ms, flip angle = 90°, acquisition matrix = 64 × 64, slice thickness = 2.4 mm, and total scan time = 16.5 min. All patients were asked to relax and keep their eyes closed and think nothing in particular during the rsfMRI scanning process. The raw data or processed data in this study will be made available to access upon a reasonable request.

## 2.3. Image preprocessing

DPARSF 4.3 (<http://rfmri.org/dpabi>; [52]) was used for the preprocessing of the rsfMRI data. For each subject, the first 10 time points were discarded. The remaining 320 volumes were first corrected for the time difference between slices and then realigned to the middle volume for head-motion correction. Skull stripping was performed for a proper registration of functional images to T1-weighted images. Head movement was corrected using motion scrubbing. The resulting images were segmented into grey matter (GM), white matter (WM), and cerebrospinal fluid (CSF), then mean BOLD signal was calculated from WM, CSF, and global signals (which is extracted from all voxels of the entire MRI volume) were regressed on the rsfMRI data. Using the normalization parameters estimated by the T1 structural image, the realigned functional volumes (voxel size [3,3,3]) were spatially normalized to the Montreal Neurological Institute (MNI) space. Then using a Gaussian kernel (FWHM = 8 mm), the dataset was smoothed, linearly detrended, and temporally filtered (0.01–0.08 Hz) to decrease the effect of low-frequency drifts. Using Automated Anatomical Labeling (AAL) atlas [53], the volumes were segmented into 90 anatomical regions of interest (ROIs) to extract the ROIs time series. The mean time series of all voxels within the ROIs were used for the connectivity analysis.

To further minimize the effects of head motion, it was estimated with Friston 24-parameter correction [52] using autoregressive models of motion by DPABI toolbox, which incorporates 12 head motion parameters for the last two time points (each of six parameters) and the 12 corresponding squared items. It also provides voxel-specific head motion calculation and correction at the individual level. We used frame-wise displacement (FD) measure for scrubbing at the quality control step [52]. This measure calculates the sum of the absolute values of the differentiated realignment estimates at every timepoint [54]. We removed volumes with FD > 0.3 mm to control head motion.

## 2.4. Simulations of synthetic data

For validation of the proposed spatiotemporal self-organizing maps

(STSOM) clustering approach and group-wise analysis, we used MATLAB toolbox, SimTB framework (<http://mialab.mrn.org/software/simtb/>; [55]) to simulate fMRI data assuming dynamic neural connectivity. Ten virtual themes have been used to form the group. Because we used the AAL atlas for real data, we also used available reported AAL atlas-based RSNs for simulate synthetic data. these RSNs including; DMN, ATN, VSN, and SMN [56,57]. For each virtual subject, time series (TS) associated with any of 90 anatomical AAL nodes were generated by applying a random variation on a 4 base template related to 4 different networks (320 time points; TR = 3s; similar to the actual fMRI acquisition parameters).

Each of 90 TSs was located to one of the 4 networks as follows; DMN (34 TS), ATN (24 TS), VSN (16 TS), and SMN(16 TS). After generation of TCs for all subjects, we added different levels of Gaussian noise,  $n(t)$ , to the time series to evaluate our proposed method as follow:

$$f(t) = S(t) + \lambda n(t) \quad (1)$$

where  $S(t)$  is the simulated time series with the mean and the standard deviation of  $\pm 0.06$  and  $0.66$ – $0.8$ , respectively.  $n(t)$  is a white Gaussian noise with the mean of 0 and standard deviation of 1 and  $\lambda$ , is a coefficient that controls the level of Gaussian noise. It was tested at levels of  $\lambda = 0.2, 0.3, \text{ and } 0.5$ , [27], representing high, medium, and low SNR, respectively.

## 2.5. Construction of group networks

Using the AAL atlas [53], 90 ROI averaged time series were extracted, and using Pearson’s correlation, a  $90 \times 90$  correlation matrix was calculated. Fisher z-transformation [58] was applied to FC matrices to improve normality for group-level comparisons. In the group clustering stage, a normal healthy group was used. The resulting cluster map represented the underlying networks among groups of individuals. Group clustering consisted of 3 steps: clustering each subject by STSOM method to obtain an individual network (step 1, Fig. 1A), applying the restricted Frechet mean method to find the mean SOM among the group (step 2, Fig. 1B), and matching the labels obtained in each subject using the mean SOM and obtain group-level networks (step 3, Fig. 1C).

### 2.5.1. Step.1: computation of individual-subject networks using STSOM

SOM is a two-layer artificial neural network that maps high-dimensional input data into a set of nodes arranged in a low-dimensional (often 2D) lattice [49]. Each SOM node has a weight vector with dimensions similar to the input vector. The SOM output is a regular two-dimensional map consisting of nodes called neurons, each connected to its neighbors. The SOM algorithm consists of a series of training steps that use unsupervised learning to adjust the weight vectors of the nodes to input vectors. At the end of the training process, a trained SOM represents the data structure in a 2D lattice [49]. In our application, we used SOM method to detect nodes’ topology in brain AAL atlas and identified functional networks as various subsets of nodes with a small within-distance and a large between-distance with other subsets.

For each subject, a  $90 \times 90$  matrix  $X$  (related to 90 AAL ROIs) containing Fisher-transformed correlation coefficients was considered as the input to the SOM. For eachmatrix element  $X_{n,i}$ ,  $n = 1, \dots, 90$  corresponds to a data point and  $i = 1, \dots, 90$  corresponds to a connectivity value (Fig. 1A). For STSOM clustering analysis, we proposed to feed the SOM with a spatiotemporal feature matrix consist of correlation coefficients as temporal attributes; and MNI coordinates of the nodes in AAL atlas as spatial attributes.

There is a consensus among the neuroscientists that the brain networks function interhemispherically symmetric in general [23,24,29,59]. We imposed this property as a constraint by considering the absolute values of the x-components in AAL coordinates (originally positive on the right and negative on the left brain hemispheres). Considering

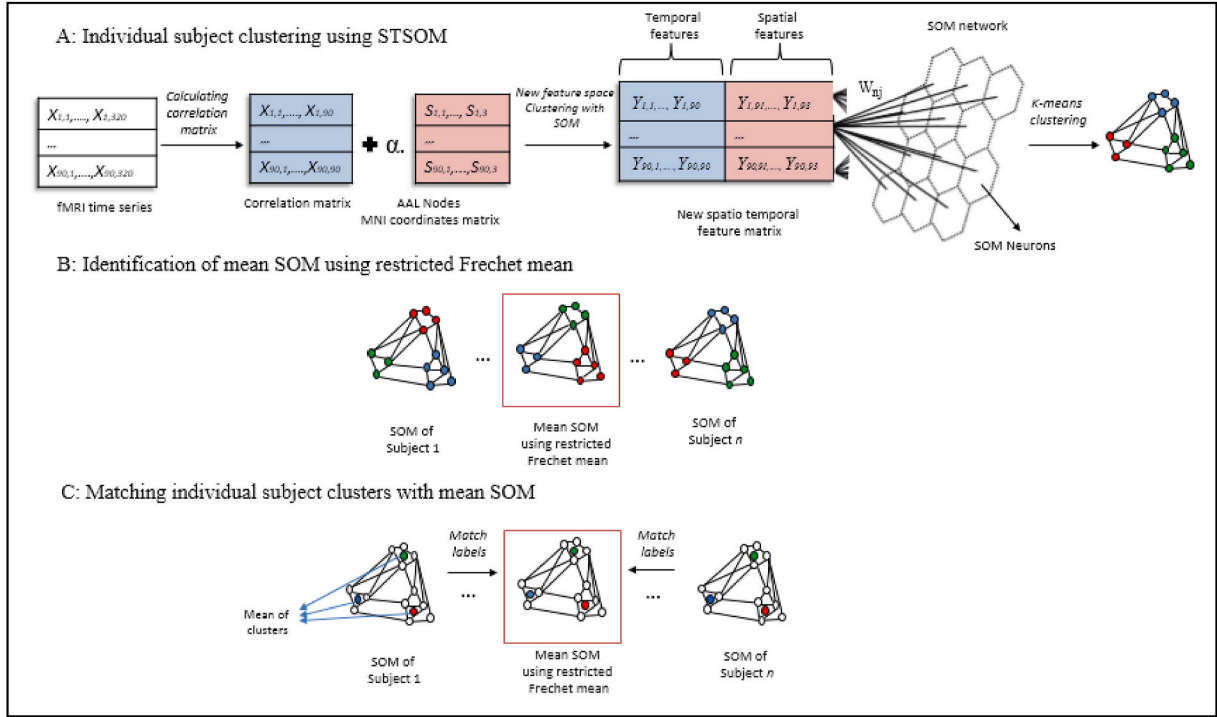


**Fig. 1.** STSOM group-wise functional network processing. A: Clustering each subject using STSOM method by combining correlation matrix and MNI coordinates of each region and obtaining an individual network. The k-means method clusters SOM results. B: Applying restricted Fréchet mean method finds the mean SOM. C: Matching the mean cluster labels of each subject with the resulted mean SOMs.

MNI location of nodes as  $S_{n,k}$  ( $n = 1, \dots, 90$ ;  $k = 1, 2$  and  $3$ , defining  $x, y$ , and  $z$  coordinates of the related node), a new input vector for each node can be represented as follow:

$$Y = \{X|\alpha.S\} \quad (2)$$

where  $\alpha$  is a regularization parameter for controlling the effect of the spatial term. As Fig. 1A illustrates, we applied the input vector  $Y$  containing spatial as well as temporal properties to the SOM for extracting functional networks. Therefore, the SOM further weights the voxels with similar temporal correlations that are closer together in the MNI space.

Each input node  $n$  is connected to each SOM neuron represented by  $j$  ( $j = 1, \dots, p$ : the total number of neurons) (Fig. 1A). The network weight,  $W_{nj}(t)$  (randomly initialized), adaptively changes at each iteration  $t$ , until convergence is reached when the distance between the input data  $Y_n$  and the weights  $W_{nj}(t)$  is minimized using equation (3).

$$d_{nj} = \sum_{j=1}^m (Y_n - W_j(t))^2 \quad (3)$$

where  $m$  is the number of neurons. The neuron with a minimum distance from an input vector (with minimum  $d_{nj}(t)$ ) is chosen as the winner and named the best matching unit (BMU). These neurons have the strongest response in the next phase. In the learning phase, the BMU and its neighboring neurons are drawn to the input vector as:

$$W_{nj}(t+1) = W_{nj}(t) + \eta(t)(Y_n - W_j(t))Z_j \quad (4)$$

where  $\eta(t)$  denotes the learning rate and  $Z_j$  is a neighborhood function. Here, we use a standard Gaussian kernel as the neighborhood function, which is commonly used to account for the effect of its neighbor values on each unit.

$$Z_j(t) = \exp(-r_d - r_c^2 / 2\sigma(t)) \quad (5)$$

where  $r_d$  and  $r_c$  are the coordinates of the neighboring and closest exemplars, respectively, and  $\sigma(t)$  controls the width of Gaussian function,

initially set to a large set of neurons and decreases to just one neuron in the final step. The learning rate is usually set larger in the early stages of the learning process and decreases as convergence is achieved. We used 100 iterations for rough-tuning (large neighborhood radius) and 1000 iterations for fine-tuning (neighborhood radius is one neuron) phases.

One of the critical parameters in SOM is the number of neurons or map size. A too-large choice leads to too-detailed patterns; while a too-small map leads to too-general patterns. In both cases, natural clusters of data cannot be adequately defined. The optimal number of neurons (the map size) is calculated as  $5\sqrt{n}$ , where  $n$  is the number of data points [60]. In our study, this optimal map size was set to 45.

Since there is not any rigid boundary between the neurons that define the clusters by SOM, the subset of neurons that are related to the set of clusters cannot be determined [61]. We used the k-means method for clustering SOM results proven to be efficient in such applications [62, 63]. There are several methods used for evaluating clusters in previous studies, such as Davies–Bouldin index (DBI) [64], Silhouette [65] and Elbow [66]. We also used the DBI, as a metric for evaluating the number of clusters. It is indeed a well-known clustering quality measure calculated by averaging the maximal similarity between each cluster and all other clusters. A higher clustering performance is associated with a smaller index. The DBI method is the most common method for determining the number of clusters in SOM-based analyzes [67–70] which is used by the SOM toolbox to determine the appropriate number of clusters. For each group, we evaluated the number of clusters as  $K$  (from 1 to 10) and we applied DBI for each subject. We considered the mean value of all subjects in the group as a group evaluation. For stability of the clustering result, we applied k-means 150 times with different initialization to detect the best clustering by the minimum within-class distance. By which, k-means clustering was used to label the SOM nodes in our application. The mean Time series of the nodes with a same label were considered for group analysis (SOM Toolbox 2.0; free download at <http://www.cis.hut.fi/projects/somtoolbox/> for MATLAB).

### 2.5.2. Step.2: identification of mean SOM using restricted Frechet mean

After applying the clustering method for individual-level networks analysis, the clustering showed no constant label numbers across the subjects. Hence, we performed a two-step approach for the detection of group cluster networks. The first step was to define the reference SOM map using a restricted Frechet mean method [51] in each group (Fig. 1B); and the second step was to match the cluster labels for individual subjects (Fig. 1C).

Since in our proposed method the data and clusters are represented by SOM networks, we used the method presented in Ref. [51], which is based on the Frechet mean method, where the mean SOM is determined and the other clusters are matched with the mean SOM clusters. SOM Frechet mean is a method to determine the reference SOM in a group of SOMs according to the SOM space measurement criterion [51]. After applying STSOM method to the individual subject, each dataset was summarized as an array of SOM map unites,  $M_q$  (with  $q = 1, \dots, v$ ) corresponding to the SOM of the  $q^{\text{th}}$  subject and total  $v$  subject. Given such a sample of SOMs,  $\bar{M}$  can then define the restricted Frechet mean:

$$\bar{M} = \arg \min_{M' \in \Lambda} \sum_{q=1}^v d(M_q, M')^2 \quad (6)$$

where  $\Lambda$  denotes the sampled  $v$  SOMs, such that  $\Lambda = \{M_1, \dots, M_v\}$  and  $d$  is the distance function as the sum of minimum distance (SMD). We used temporal SMD (T-SMD) to deal with the problem of comparing multiple SOMs [71]. Given two sets of SOMs denoted by  $M_x$  and  $M_y$ , the SMD can be computed as follow.

$$d(M_x, M_y) = \frac{1}{2V} \left( \sum_{W_x \in M_x} d_e(W_x, M_y) + \sum_{W_y \in M_y} d_e(W_y, M_x) \right) \quad (7)$$

where  $V$  is the total number of input vectors,  $d_e$  is the Euclidean distance.  $W_x$  and  $W_y$  are the weight vectors of every neuron of  $M_x$  and  $M_y$ , respectively. After specifying the reference SOM, the clusters of individual subjects can be arranged.

### 2.5.3. Step.3: matching individual subject clusters to find group networks

After obtaining the reference SOM, we used the mean of the neurons in each cluster as a representative to match the clusters to reduce the effect of outlier data and also the computational complexity. To match clusters of each individual subject, we considered all possible cluster matchings between cluster means-using all possible cluster permutations- and calculate the overall similarity value as the sum of similarity values for all matched clusters. The overall best match was the permutation maximizing the global similarity based on the Euclidean distance between the two clusters.

### 2.6. Labeling the functional networks

Networks were assigned by calculating the Hausdorff distance between each detected network and the known major functional brain networks computed for a large number of subjects [23,24,59]. The Hausdorff distance is a dissimilarity measure that represents how far two regions are from each other and is defined as follow:

$$HD = \max(h(A, B), h(B, A)) \quad (8)$$

$$h(A, B) = \max_{a \in A} \left\{ \min_{b \in B} \{d(a, b)\} \right\} \quad (9)$$

where  $A$  and  $B$  are two sample sets and  $d(a, b)$  denotes the Euclidean distance between  $a$  and  $b$  as points of  $A$  and  $B$ , respectively. The Hausdorff distance is more sensitive to outliers than other methods like Dice's coefficient and Jaccard distance in measuring the closeness of two sets. It also is not sensitive to the size of clusters which makes it suitable for comparison between brain networks. We also used it for evaluating our

proposed results in the syntactic data set.

### 2.7. Network quantification

After obtaining the functional networks, the ROIs of each network were put together and the connectivity matrix was calculated using the Pearson correlation between each node time series. The Fisher Z transform [58] was then applied to the correlation matrix. The average FC of the within and between-network connectivity for each network were computed and then these measures were compared across three HC, LTLE and RTLE groups using one-way ANOVA. Bonferroni correction (with 3 tests) was applied to adjust for multiple comparisons.

To investigate the generalizability of the obtained functional network to other controls the control subjects were divided into two groups (5 and 6) with a surrogate and a samples  $t$ -test was used to compare the two groups. Samples  $t$ -test is a suitable method of testing hypotheses about the mean of a small sample population when the population standard deviation is unknown.

### 2.8. Identification of regularization parameter $\alpha$

As mentioned in Section 2.5.1, we considered each row of the Fisher-transformed connectivity matrix for each subject as a data point. As shown in Fig. 1, for each node, the MNI coordinates of the corresponding node were added as three new spatial features to the 90 functional features (90 connectivity values corresponding to each node). We used a homogeneity measure to evaluate the effect of  $\alpha$  parameter on the simulated and real data. A functional network should not only be distinct from other networks, it also should maintain a uniform and consistent connection pattern across its nodes. In other words, the connections of a functional network should be homogeneous within it. Therefore, a degree of homogeneity for the created networks can be considered as a quantitative criterion for the functionality of the networks. We used this as a ground to investigate the effect of the alpha parameter in determining the optimal networks [26,27]. The homogeneity of the clustering was assessed using the following technique: For each network, we computed the average z-transformed correlations within a network. Then, these values were averaged across all resulted networks for each subject. Finally, the resulted values were averaged across all subjects [26].

We also used a homogeneity measure to compare the performance of our proposed network with two standard functional networks, namely the Power and the Yeo networks. Since the degree of homogeneity is related to the network size, any assessment of the homogeneity in any network should be through a comparison to a null model - to decide whether it is more homogeneous than expectedly random networks of a similar size [72]. Therefore, we evaluated the degree of homogeneity for each network under the study with many random networks of the same size through the random placement of nodes in each network.

## 3. Results

### 3.1. Head motion correction

All the subjects were checked for head motion; the mean displacement was  $<3$  mm and the mean rotation was  $<3^\circ$ . There was no significant difference in mean head motion between groups based on the subject-averaged framewise displacement (FD) measurement [11]: HC =  $0.112 \pm 0.033$  mm; LTLE =  $0.124 \pm 0.040$  mm; RTLE =  $0.128 \pm 0.047$  mm; ANOVA test:  $F(2, 46) = 1.28$ ;  $P = 0.28$ .

### 3.2. Result of synthetic data

STSOM clustering algorithm and the restricted Frechet mean methods were applied to the synthetic data. Fig. 2A shows the surface map of the DBI for different values of  $\alpha$  from 0 to 1. As Fig. 2B shows, for

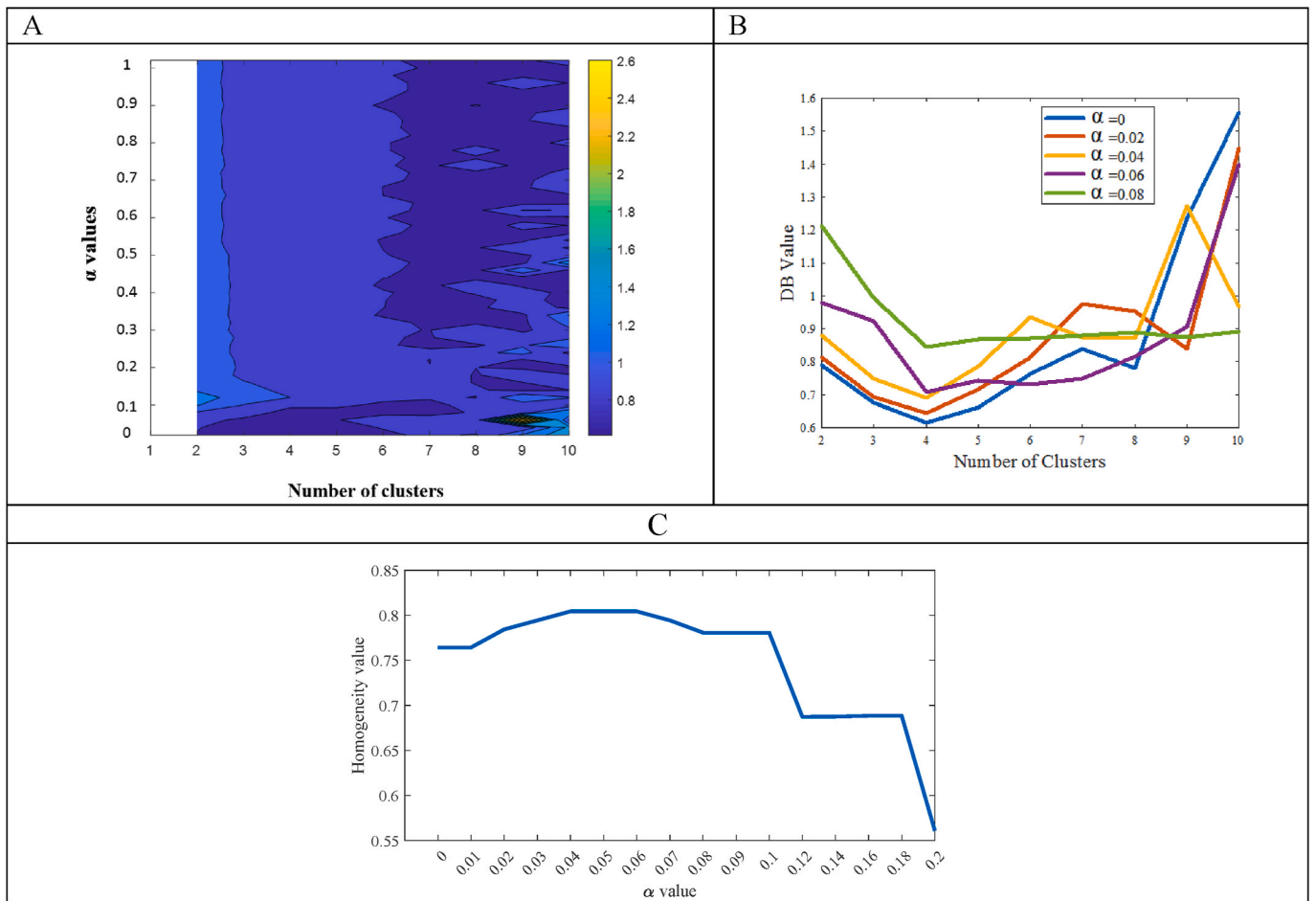


Fig. 2. A: Surface map of the DBI for different values of  $\alpha$  from 0 to 1. B: DBI for different values of  $\alpha$  from 0 to 0.08. C: Homogeneity measures for different values of  $\alpha$  between 0 and 0.2. X and y axes show the cluster number and  $\alpha$  values from 0 to 1, respectively.

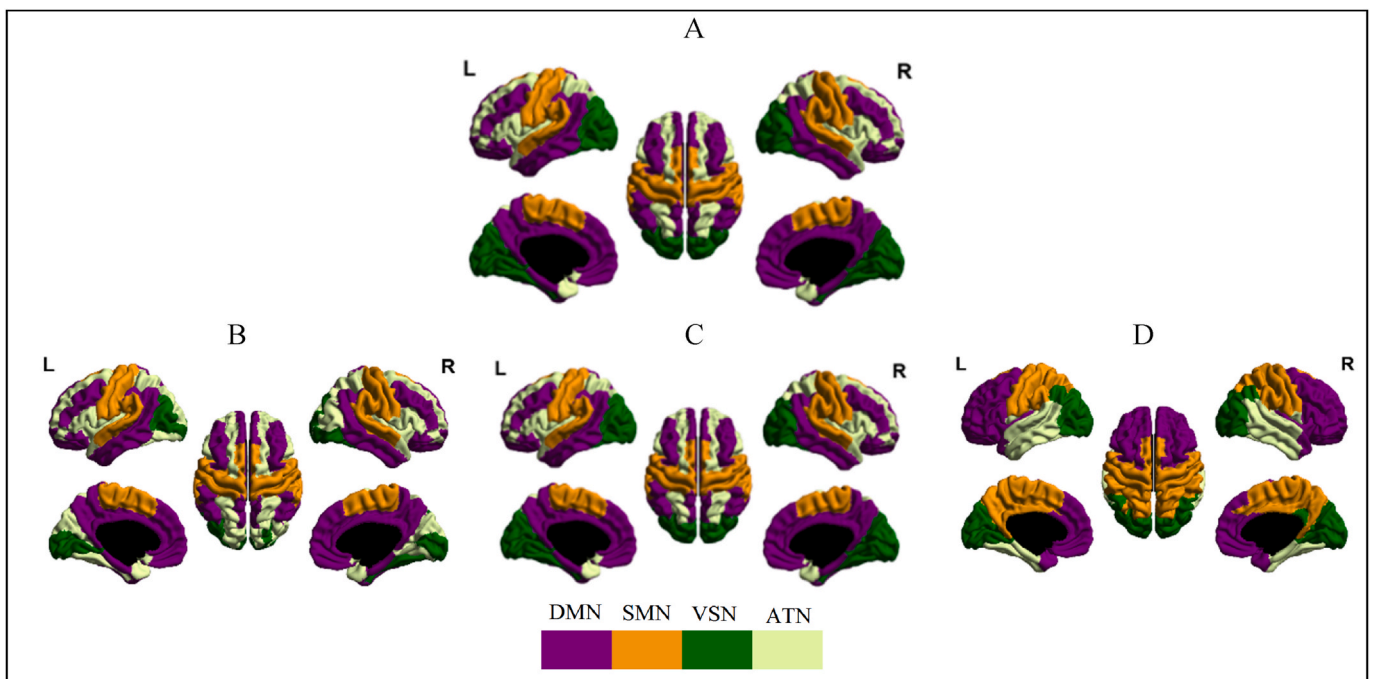


Fig. 3. Effect of regularization parameter  $\alpha$  on the resulted networks for simulated fMRI data, A: simulated networks, B:  $\alpha = 0$ ; related to no regularization, C:  $\alpha = 0.05$ , related to optimal a decent regularization based on homogeneity measures analysis and D:  $\alpha > 0.1$ ; related to high regularization of the spatial parameter.

small values of  $\alpha$  ( $\alpha < 0.1$ ), an appropriate number of clusters is achieved 4. Fig. 2C shows the result of homogeneity measures for different values of  $\alpha$  between 0 and 0.2. This figure shows the homogeneity values are maximum for  $\alpha$  values of 0.04, 0.05, and 0.06. we tested these values and no differences were achieved in the resulted networks. Therefore, we chose  $\alpha = 0.05$  for further analyses.

To investigate the effect of regularization parameter  $\alpha$  on the resulted networks, the networks were obtained for  $\alpha$  values of 0 (no regularization), 0.05 (optimal regularization based on homogeneity measures analysis) and  $\alpha > 0.1$ , (a high regularization of the spatial parameter) (Fig. 3). As illustrated by Fig. 3B the VSN network is not delineated correctly and the FPN network has overlapping with visual area. Fig. 3C, demonstrates that with the optimal value of the  $\alpha$  parameter, all 4 networks are correctly delineated. As Fig. 3D shows, as the effect of a high spatial parameter, each network is concentrated in one area. For example, in the frontal region, only the DMN network is identified. In addition, the motor network has extended to parietal regions.

Fig. 4 shows a parcellation using STSOM compared with the conventional SOM. The difference is exploiting the restricted Frechet mean method for group analysis (named SOM1) and applying the conventional SOM on an averaged connectivity matrix (named SOM2) at different SNR values. Fig. 5 also shows the Hausdorff distance between each pair of resulted networks by three mentioned methods and pre-defined simulated networks for a different level of SNR.

As Fig. 4 shows for  $\lambda = 0.2$ , STSOM and SOM1 methods performed well for quite high values of SNR but missed clustering was observed in the SOM2 method in the visual and attention networks. The Hausdorff distance reached lower values in STSOM and SOM1 methods and larger values in the SOM2 method (regarding misidentifying of visual and attention networks) (Fig. 5A). As the noise level was amplified with  $\lambda = 0.3$ , the SOM2 failed to detect networks and the SOM1 also started to fail. However, Fig. 4 shows that the STSOM approach was able to correctly identify all four regions. The Hausdorff distance also reached low values in STSOM and large values in SOM1 (related to visual network) and SOM2 (related to visual and attention networks) methods (Fig. 5B). At the lowest SNR level ( $\lambda = 0.5$ ), the STSOM method was still able to parcellate all 4 regions, while the conventional SOM with restricted Frechet mean and also simple averaging failed to define four functional networks correctly. As shown in Fig. 4C STSOM method resulted in a low Hausdorff distance. Both SOM1 and especially SOM2 show a large Hausdorff distance for all networks.

### 3.3. Resting-state functional networks

In the previous section, the comparison of the proposed spatiotemporal clustering algorithm STSOM and the conventional SOM approaches demonstrated that the STSOM was capable to produce more accurate and more robust parcellation results compared with SOM1 and

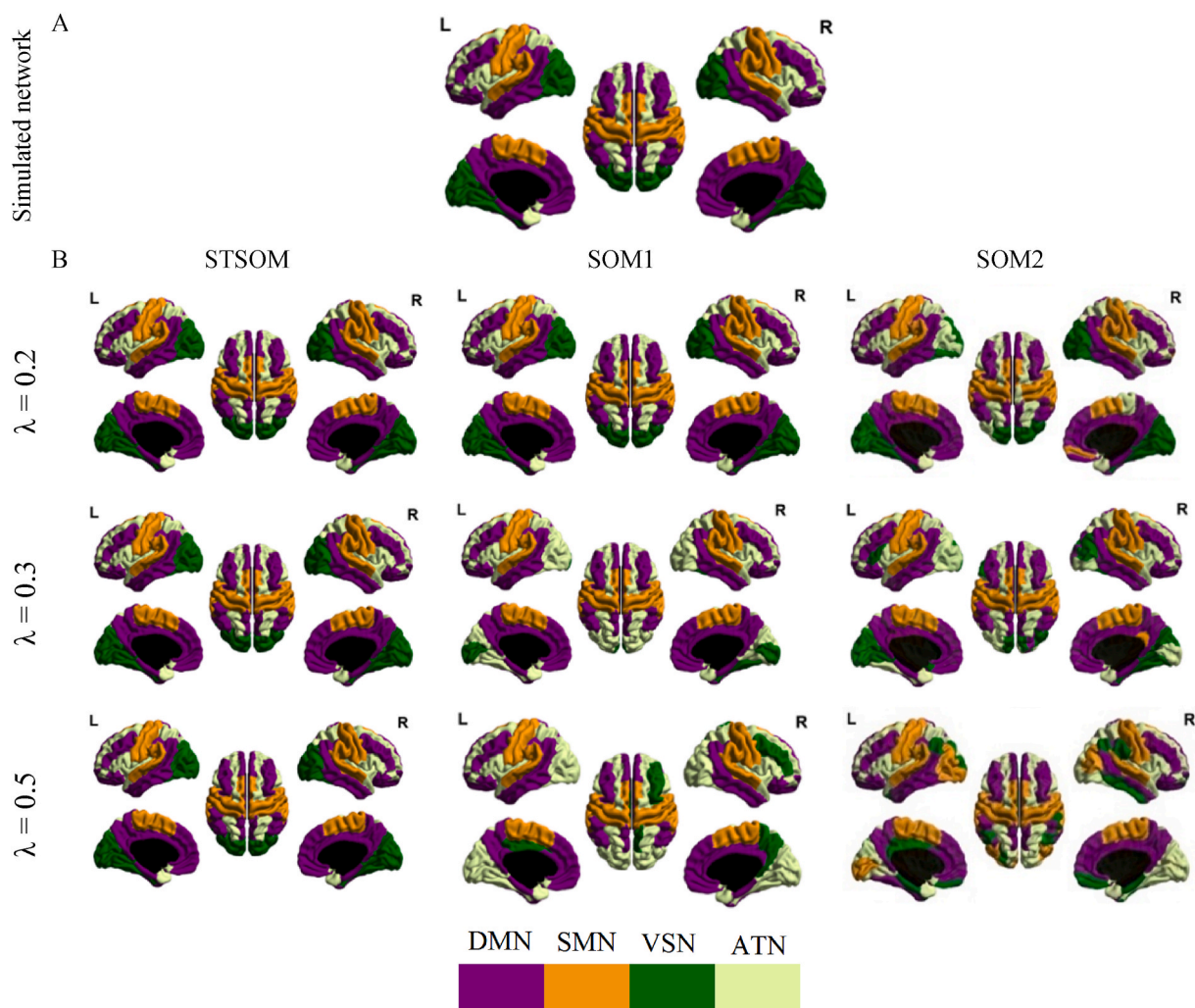


Fig. 4. Comparing the resulted networks by proposed STSOM method A: Gold standard simulated networks. B: Result of proposed STSOM method, conventional SOM using restricted Frechet mean method (SOM1), and without restricted Frechet mean using a simple averaging connectivity matrix (SOM2).  $\lambda$  represents the level of Gaussian noise. (For interpretation of the references to color in this figure legend, the reader is referred to the Web version of this article.)

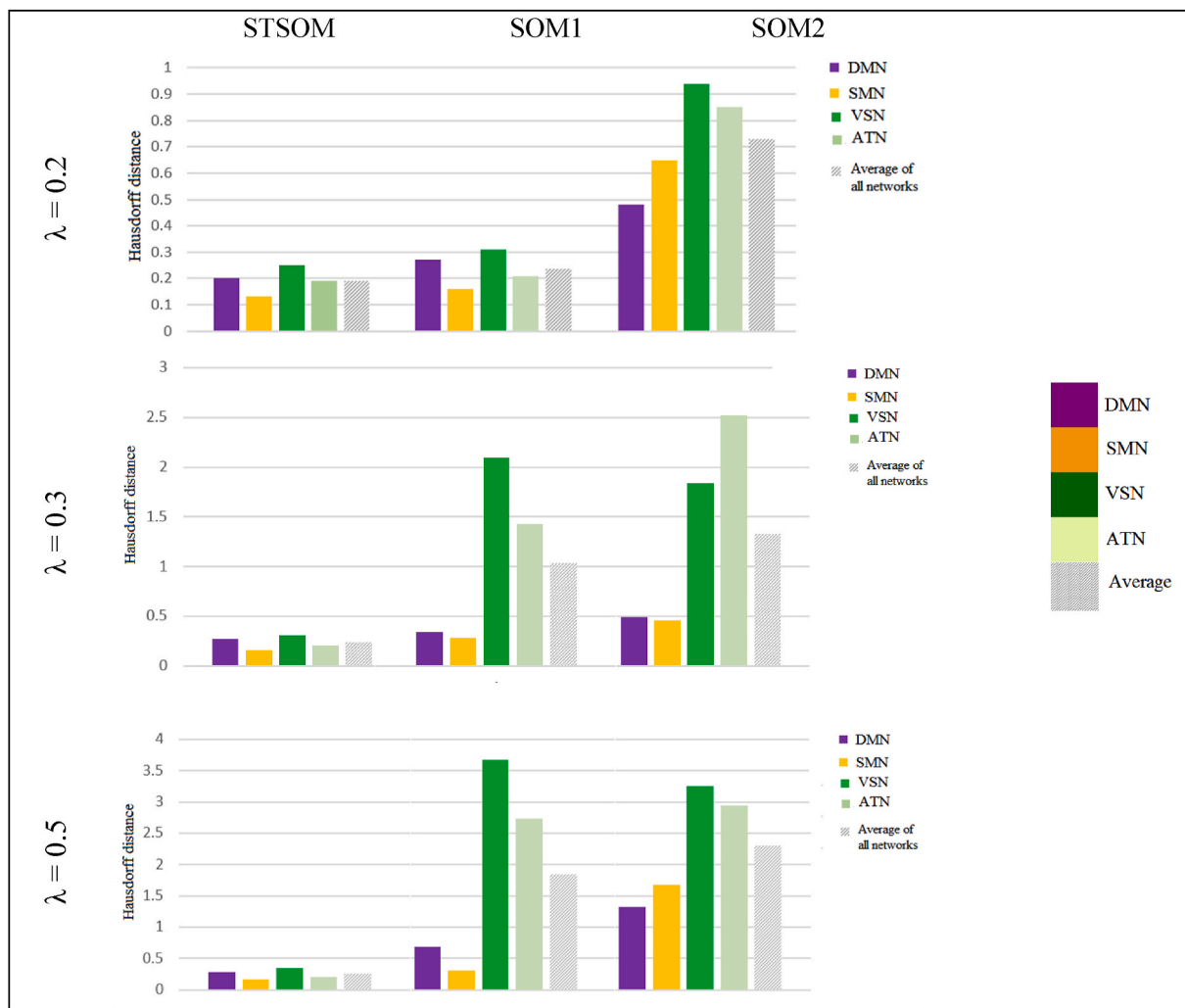


Fig. 5. The Hausdorff distance between each pair of resulted networks and predefined simulated networks. Proposed STSOM method with conventional SOM using restricted Frechet mean method (SOM1), without restricted Frechet mean using a simple averaging connectivity matrix (SOM2).  $\lambda$  represents the level of Gaussian noise.

SOM2 methods for a range of SNR values.

The number of clusters was specified using the DBI. A surface map for  $\alpha$  values between 0 and 1 is generated and shown in Fig. 6. As can be seen in this figure, for 8 clusters, the value of DBI is minimal for all  $\alpha$  values as well as in all three HC, LTLE and RTLE groups. This means that the 8 networks seem to be optimal. Fig. 6B represented homogeneity measures for different  $\alpha$  values. As this figure shows, the homogeneity measures were almost maximum for 0.04, 0.05 and 0.06. We tested these 3 values and the resulting networks did not differ, so we set  $\alpha$  parameter to 0.05.

Fig. 7 shows the obtained networks for  $\alpha$  values of 0 and 0.05, for 8 networks. Note that for  $\alpha = 0$  (without spatial and hemisphere symmetry effect), the resulting networks are neither regular nor symmetric, but  $\alpha = 0.05$  generated almost symmetric networks.

The overlap ratio concerning the Hausdorff distance between each HC individual's consensus network and previously defined reference networks is shown in Tables S1–S3. As Tables S1–S3 shows networks 1 and 2 had a minimum Hausdorff distance with DMN in all three atlases. Considering this criterion and also the visual comparison of networks with three standard functional atlases, we combined networks 1 and 2 to define the default mode network (DMN). Networks 3 and 4 were the shortest distance from SMN and VSN, respectively, in all 3 atlases, therefore they were also considered as SMN and VSN. The results of the brain cortical visualization also validated this specification. Network 6

had the shortest distance to SCN in the AAL based atlas [43], to DMN in Yeo atlas, and to DMN and SCN networks in Power atlases. Since we used AAL atlas, we considered this network as SCN. The results of the visualization networks on the brain cortex also validated this dedication. The remaining 5,7 and 8 networks were considered as DAN, FPN, and VAN, respectively, according to the Hausdorff distance and visual inspection on the cortex. The results of applying our proposed method revealed 8 networks in the HC subjects that are described with different colors on the cortical surface shown in Fig. 8A. The final 7 data-driven functional networks on the cortical surface are shown in Fig. 8. B, consisting DMN, SMN, VSN, SCN, FPN, DAN, VAN. We also visualized Yeo 2011 and Power networks that were overlayed on AAL atlas for comparison with our proposed networks in Fig. 9.

### 3.4. Homogeneity measures for different methods and null model

Fig. 10 represents the homogeneity measures calculated for our STSOM proposed method and also for Power and Yeo methods. As this figure shows, the STSOM method also achieved a larger homogeneity value compared to both Power and Yeo methods. In addition, all three methods exhibited a larger homogeneity compared to their corresponding null model.

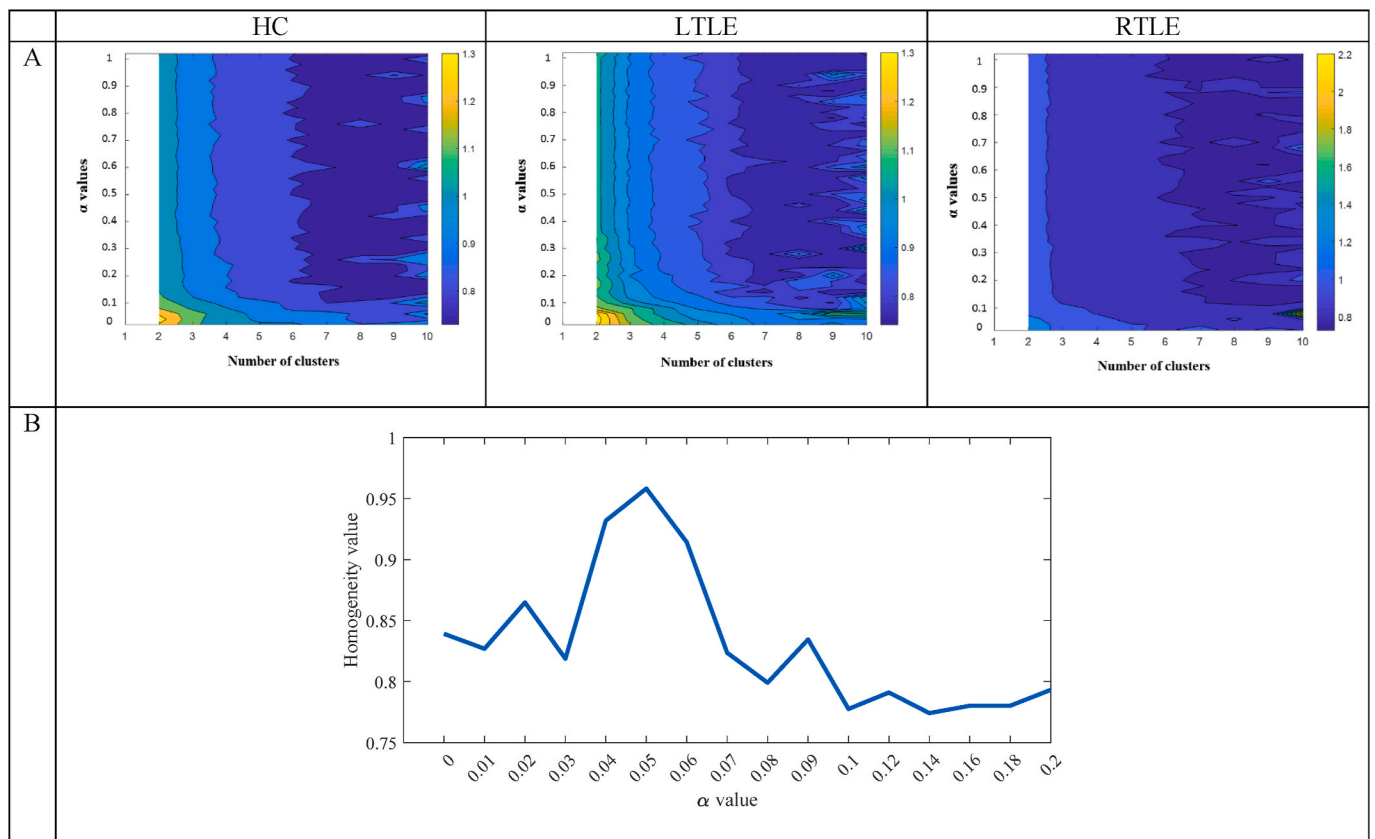


Fig. 6. A: Surface map of DBI for different values of  $\alpha$  parameter for normal group (HC), left-TLE group (LTLE) and right-TLE group (RTLE). x axis shows the cluster number and y axis shows  $\alpha$  values from 0 to 1. B: Homogeneity measures for different  $\alpha$  values between 0 and 0.2.

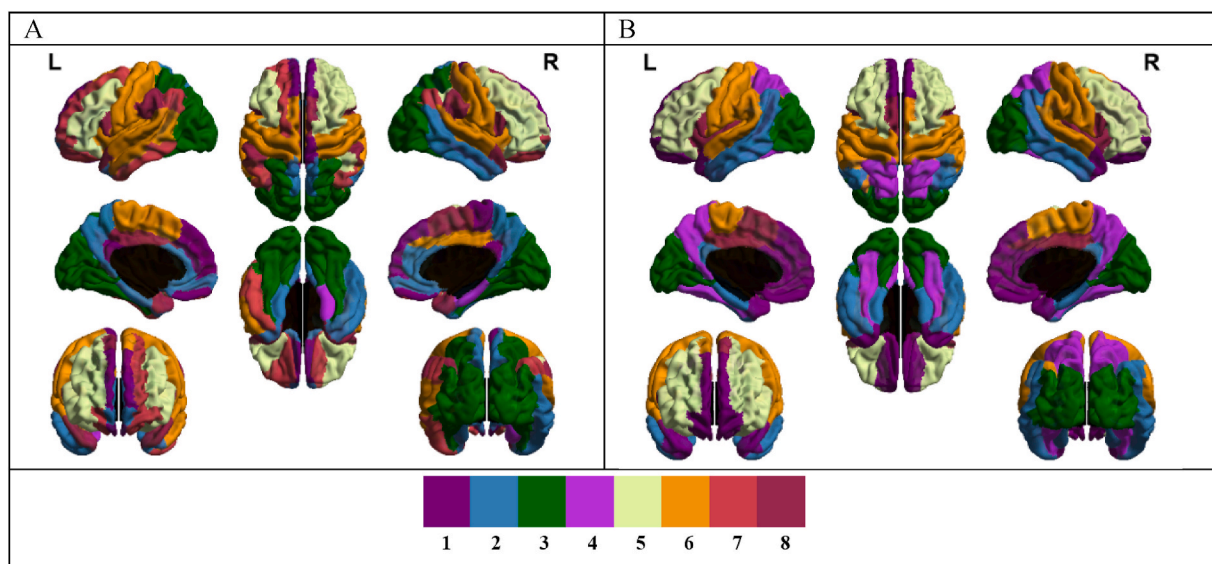


Fig. 7. Visualization of the data-driven brain networks by the proposed method. A: 8 resulted networks using  $\alpha = 0$  (without spatial and hemispheric symmetry properties) B: 8 resulted networks using  $\alpha = 0.05$ .

### 3.5. Brain network connectivity alterations in MTLTLE

For evaluation of the reproducibility of the proposed method on different datasets, we compared the 5 control groups to another 6 control groups. There were no significant differences detected between these groups (samples *t*-test,  $p > 0.05$ ) on average FC of the within-network and between-network connectivity. The averaged functional

connectivity matrix for each of HC, LTLE, and RTLE groups are shown in Fig. 11A and the averaged within and between network connectivity matrix is shown in Fig. 11. B.

Significantly increased within-network FC in FPN and DMN (Bonferroni corrected  $p < 0.05$ ) were seen in LTLE group compared to HC group (Fig. 12). Both LTLE vs. RTLE and RTLE vs. HC groups showed no significant within-network FC difference in any of the RSNs. A

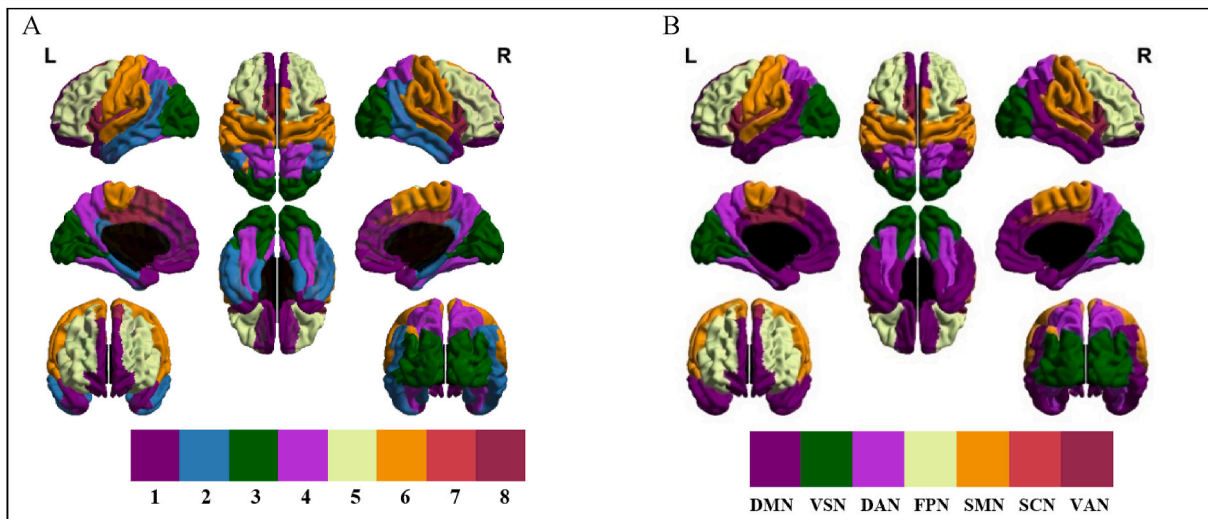


**Fig. 8.** Visualization of the data-driven brain networks by the proposed method. A: the 8 raw data-driven networks B: final 7 labeled networks. (1) Default-mode Network (DMN), (2) Sensorimotor Network (SMN), (3) Visual Network (VSN), (4) Subcortical Network (SCN), (5) Frontoparietal Network (FPN), (6) Dorsal attention Network (DAN), (7) Ventral attention Network (VAN).

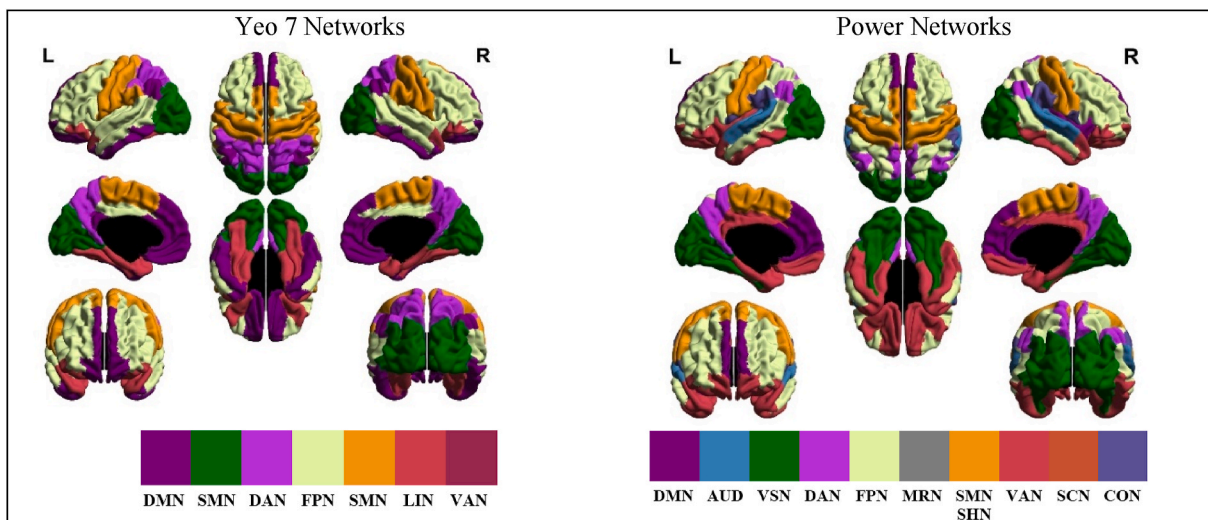


**Fig. 9.** Visualization of Yeo 2011 and Power 2011 resting-state networks overlaid on AAL atlas (1) Default-mode Network (DMN), (2) Sensorimotor Network (SMN), (3) Visual Network (VSN), (4) Subcortical Network (SCN), (5) Frontoparietal Network (FPN), (6) Dorsal attention Network (DAN), (7) Ventral attention Network (VAN), (8) Limbic Network (LIN), (9) Auditory Network (AUN), (10) Memory retrieval Network (MRN), (11) Somatomotor Hand (SHN), (12) Cingulo-opercular Task Control (CON).

comparison of between-network FC with the HC group showed that both LTLE and RTLE cohorts showed increased FC between “DMN, FPN”. Moreover, LTLE patients showed increased FC between “DMN, VSN”, “DMN, SCN”, “DMN, FPN”, “DMN, DAN”, “FPN, VSN”, “FPN, SCN”, “FPN, DAN”, and “FPN, VAN”. Finally, no significant difference of FC between any of RSNs was detected between the LTLE and RTLE patients (Fig. 12).

To make a comparison between our proposed method with other standard methods, we assigned 90 AAL ROIs to RSNs reported by Yeo et al. [12] and Power et al. [11]. Then, we compared alteration between mTLE groups and HC group using the RSNs.

For Yeo et al. networks, as shown in Fig. 13, within-network FC increased in LIN and DAN in LTLE group compared to HC. None of the functional networks showed an increase in within-network FC in RTLE group compared to HC or LTLE cohort. Between-network FC increased between “DMN, FPN”, “DMN, LIN”, “DMN, DAN”, “DMN, VSN”, and “DAN, LIN” in LTLE cohort compared to HC. Between-network FC

increased between “DMN, LIN” in RTLE compared to HC (Bonferroni corrected  $p < 0.05$ ) (Fig. 13).

Using Power networks, we repeated the above mentioned comparisons. Within-network FC increased in DMN and DAN for LTLE cohort compared to HC. None of the functional networks showed an increase in within-network FC in RTLE group compared to HC or LTLE cohort. Between-network FC was increased between “DAN, FPN”, “DAN, VSN”, “DAN, SMN”, “DAN, SHN” and “FPN, SAN”, “FPN, VSN”, “FPN, DMN”, and also “DMN, VSN” in LTLE compared to HC; and between “DAN, SHN” and “SAN, FPN” in RTLE compared to HC (Bonferroni corrected  $p < 0.05$ ) (Fig. 13). Finally, no significant difference of FC between any of RSNs was detected between the LTLE and RTLE patients using either of Yeo and Power networks (Bonferroni corrected  $p < 0.05$ ).

#### 4. Discussion

In this study, accounting for spatial structure and hemispheric

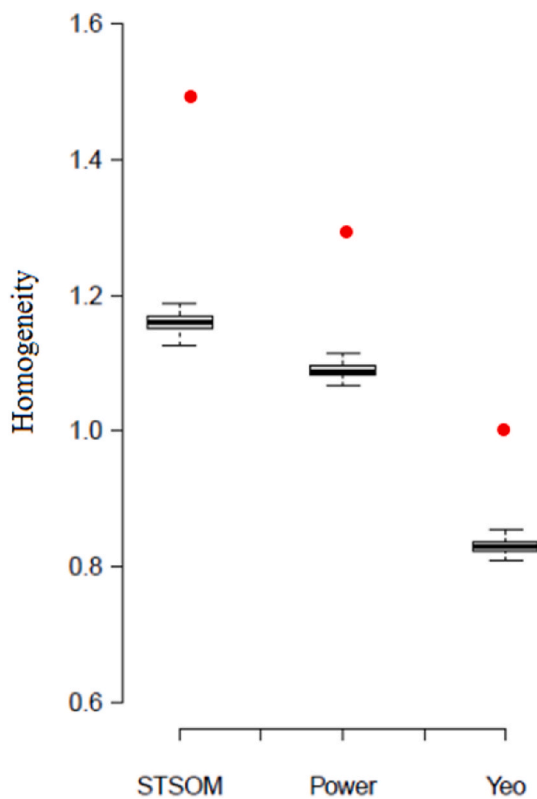


**Fig. 10.** Homogeneity measures calculated for our proposed STSOM method and Power and Yeo methods. Box plots represent homogeneity measures related to 1000 random generations of a null model. Red dots represent each method's homogeneity measures. (For interpretation of the references to color in this figure legend, the reader is referred to the Web version of this article.)

symmetry of the brain function, we proposed a clustering approach for analyzing the resting-state fMRI using a novel data-driven framework of spatiotemporal self-organizing maps and a group-level analyzing method for identifying the functional brain networks and their characterization in left and right mTLE. Specifically, it is evidenced that the brain is functionally correlated and spatially homogeneity structured. The time courses are usually noisy and contain a small set of samples compared to the spatial maps. The small sample size and inherent noise reduce the accuracy of computed statistics. In contrast, we integrated spatial and temporal information using a self-organizing map for detecting main brain networks. Our novel group-level analysis based on self-organizing maps and the restricted Fréchet mean method also demonstrated homogeneity of the identified networks. We investigated the functional networks in left and right mTLE and healthy control cohorts and compared them with the corresponding Yeo and Power functional networks. The results indicated that mTLE is characterized by a significant reorganization of frontoparietal, default-mode, and dorsal attention functional networks in mTLE. Moreover, the pattern of the altered network connectivity in the left and right mTLE patients significantly differed from the healthy controls.

This study is a pioneering resting-state study that integrates spatial information of the regions of interest into the temporal signal properties, with the assumption of hemispheric symmetry in brain functions, and exploits an SOM clustering approach to investigate the whole-brain RSNs. Compared with other methods using clustering techniques for identification of functional networks [39,40,44], applying spatial information would increase the homogeneity of identified networks and prevent the effect of noise and outliers on clustering. Spatial information was previously investigated in an ICA analysis [32], in which the strong assumption of independence of the components may deteriorate its ability to detect functional networks in real applications [46,73].

One of our aims was to obtain brain functional networks in AAL Atlas that have not been extracted before. Specifically, in Power (2011) study [23], as one of the most common functional networks in resting state analysis, the application of a graph-based method on AAL atlas does not extract the DAN, which is now well defined using our proposed method.

Another advantage of the proposed method compared to other brain functional atlases such as Power and Yeo networks, is the use of the AAL90 atlas to determine the brain functional networks. The AAL atlas is one of the most widely used atlases in resting-state fMRI analysis. However, there has been no report of using spatial information based on the AAL atlas to extract brain functional networks. Moreover, a node-based approach for analysis of the brain networks has advantages over voxel-based approaches, namely: reducing the effect of noise on functional time series, the computational burden, and the number of parameters to be estimated [27].

Exploiting regularization in extracting functional networks can ascertain the hemispheric symmetry. Recent studies reported more than 95% symmetric hemispheres in mean resting-state connectivity [29]. Only small areas like language and hand preference have shown asymmetry functional patterns [29,74,75].

The language and memory networks are within the most important networks affected by temporal lobe epilepsy, yet they manifest inter-hemispherically asymmetric properties. However, in one hand, the language and memory networks are not among the main large-scale brain networks [23,24] and identifying them requires a secondary analysis as they overlap with other large-scale networks such as FPN and DMN [76–78]. On the other hand, we enforced network symmetry by exposing a constraint on MNI coordinates of 90 nodes of AAL atlas in our proposed method, not on asymmetric properties on the large-scale networks.

Moreover, since the data of healthy people have been used in standard methods to extract functional networks [23,24,26,27], it seems acceptable to assume symmetric behaviors of the functions implemented in brain hemispheres. However, this assumption is only considered for spatial features (MNI coordinates) that are added to functional connectivity features, and the functional features are preserved to demonstrate potential functional laterality in some areas.

Different values of the regularization parameter  $\alpha$  can affect the networks identified in the simulated as well as real fMRI data. The results showed that the spatial information can extract the correct and symmetric functional networks. When there is no spatial parameter effect ( $\alpha = 0$ ), some networks (like the VSN and ATN in simulated data) are not determined correctly, and some resulted networks are not symmetric. Applying the homogeneity measure for evaluation of regularization parameter  $\alpha$  showed that the range of 0.04–0.06 would be optimal for both syntactic and real fMRI data. Since the value of functional features for each node is approximately limited between  $-2$  and  $2$  (due to Fisher transform) and also the MNI coordinates in the AAL atlas adopt the values in the range of  $-85$  to  $70$ , to match the weight of spatial and functional properties, the regularization parameter should be small and in and about 0.05. Furthermore, a small value of  $\alpha$  would guarantee to preserve the functional nature of the networks and probable inherent laterality in some functional networks.

To compare different network generating methods, since the homogeneity measure depends on the number and the size of networks, and smaller networks are inherently more homogeneous [27]. Therefore, comparing the degree of homogeneity alone may not show the superiority of a method, and the comparison should be made for each method with its null model to reflect the performance quality. We demonstrated that our method is more homogeneous than the random size and shape match null model, and also performs superior relative to its null model compared to Power and Yeo networks being overlaid on AAL atlas.

Due to the variabilities between atlases in the number and location of regions and also the difference between the average bold signals of the network regions, utilizing each atlas may lead to variable brain

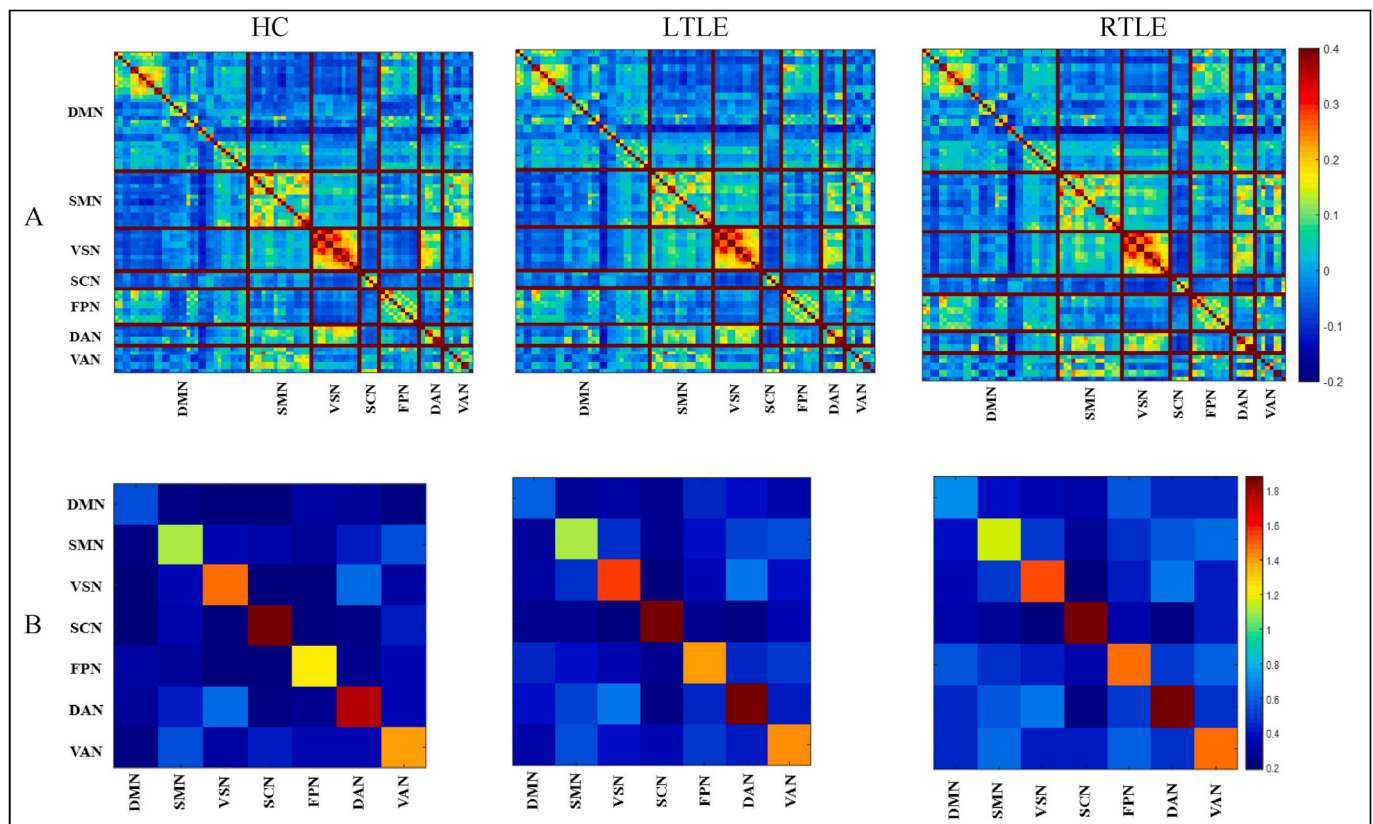


**Fig. 11.** Connectivity matrix of sorted node based on data-driven networks. A: The raw Fisher z transformed connectivity matrices for HC, Left -TLE, and right-TLE. B: The mean within and between connectivity matrices for the networks identified for HC, Left -TLE, and right-TLE. DMN: Default-mode Network, SMN: Sensorimotor Network, VSN: Visual Network, SCN: Subcortical Network, FPN: Frontoparietal Network, DAN: Dorsal attention Network, VAN: Ventral attention Network. HC: Healthy control.

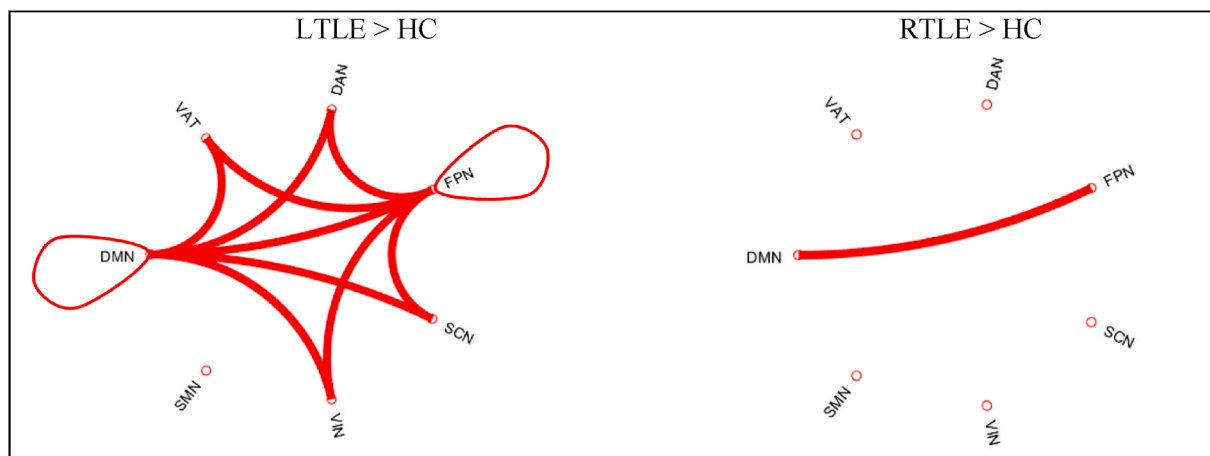


**Fig. 12.** Statistical comparison of left-TLE vs. HC and right-TLE vs. HC (Bonferroni corrected  $p < 0.05$ ). Red lines indicated significantly increased functional connectivity between networks. Lines between networks indicated between-connectivity and circle lines indicated within-connectivity networks. DMN: Default-Mode Network, SMN: Sensorimotor Network, VSN: Visual Network, SCN: Subcortical Network, FPN: Frontoparietal Network, DAN: Dorsal Attention Network, VAN: Ventral Attention Network. LTLE: Left-mTLE, RTLE: Right-mTLE, HC: Healthy control. (For interpretation of the references to color in this figure legend, the reader is referred to the Web version of this article.)

functional networks [23] with even difficult comparisons. The major existing functional networks are originally based on other atlases or voxel-based methods, and their adaptation to AAL regions require further analysis and sometimes not quite possible. In this study, we used the AAL atlas as one of the most common parcellation methods in resting-state fMRI studies to extract the functional networks. We will implement the proposed method on other atlases in future works.

Despite a previous method [44], where the number of networks and the type of networks have been chosen based on prior information taken from previous works, our proposed method has this advantage that we made no assumption about the number of networks and the network type; and obtained them merely by adopting a data-driven approach.

Another advantage of our proposed method compared with graph-based methods [23,24,79-81] that are commonly used to extract

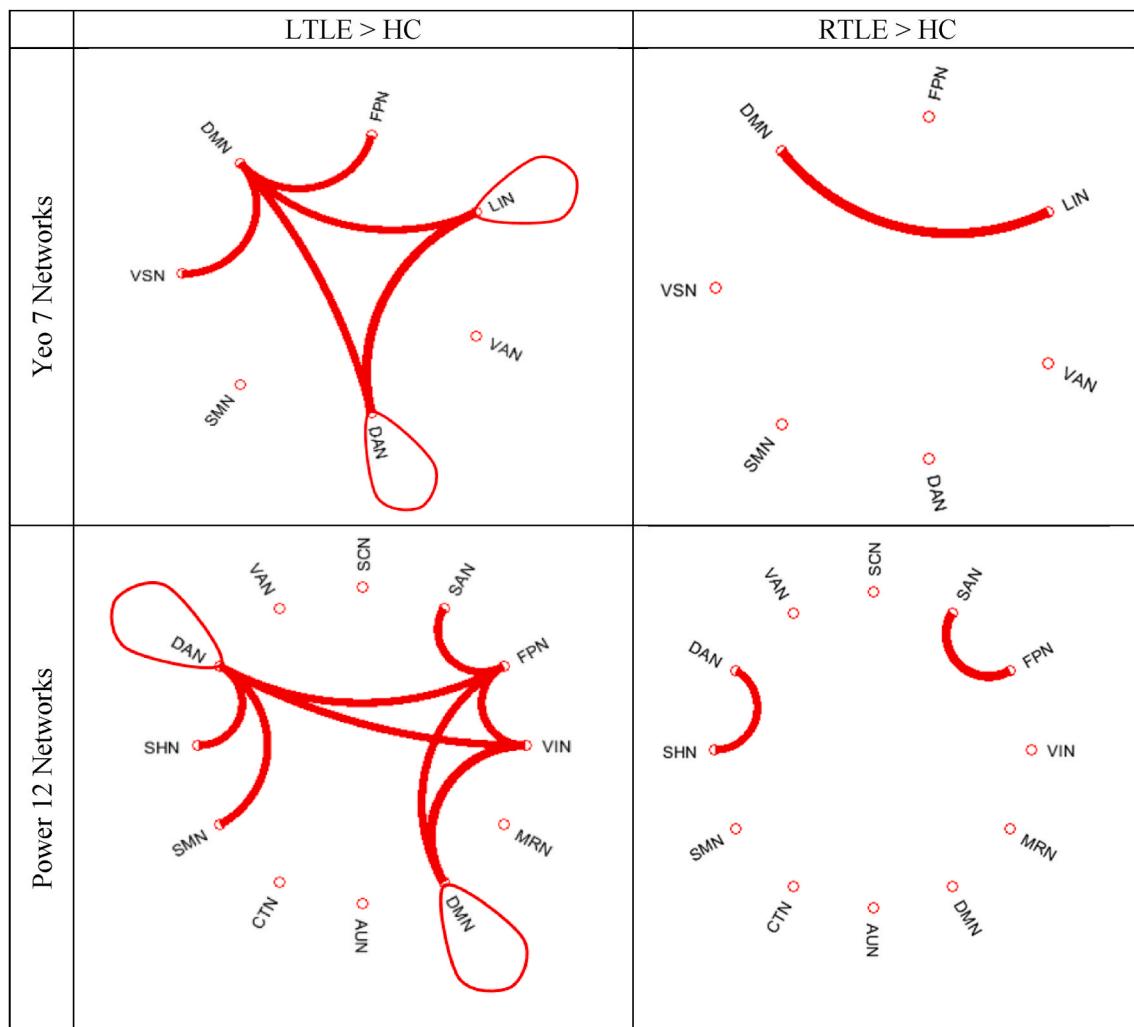


**Fig. 13.** Statistical comparison of left-TLE vs. HC and right-TLE vs. HC (Bonferroni corrected  $p < 0.05$ ) using Yeo 7 networks and Power 12 networks. Default-Mode Network (DMN), (2) Sensorimotor Network (SMN), (3) Visual Network (VSN), (4) Subcortical Network (SCN), (5) Frontoparietal Network (FPN), (6) Dorsal Attention Network (DAN), (7) Ventral Attention Network (VAN), (8) Limbic Network (LIN), (9) Auditory Network (AUN), (10) Memory Retrieval Network (MRN), (11) Somatomotor Hand Network (SHN), (12) Cingulo-Opercular Task Control Network (CON).

functional networks, is that there is no need to select any specified thresholds. Previous network clustering methods depended on applying arbitrary thresholds to the connectivity matrix in which different thresholds can lead to different network clustering results. The network community detection highly depends on network density. If no threshold is applied then the network community analysis might not be practically feasible. Since STSOM uses full networks directly for clustering and the connection size is automatically considered as a result of clustering, there is no need to applying any threshold and binarizing the networks. Thus, STSOM can eliminate the uncertainty resulting from the selection of threshold values and potentially provides a stronger and more consistent approach to research on brain networks. However, direct comparisons between STSOM and existing threshold-based techniques are beyond the scope of this study. The only parameter that should be specified in our proposed method is the regularization parameter  $\alpha$ . As shown by the results, the choice of the number of clusters does not depend on regularization parameter. Other clustering methods such as ICA, Hierarchical, N-Cut, in addition to the number of clusters, have other parameters that need to be specified.

Previous methods have mainly used the average of the functional connection matrix in a group to obtain the group representative networks. According to the sensitivity of the BOLD signal to the noise level and the possibility of inaccuracy in individual data, the final result will

be directly affected. In particular, we proposed a new and robust machine learning framework using restricted Fréchet mean for examining performance networks, which can be extracted in groups with some advantages. Using the restricted Fréchet mean method, the complexity of the group analysis method is greatly reduced, because the inference is made using group labels, and it is unclear whether such a large number of displacements is possible, limiting this to using the Fréchet constraint. On the other side, this method selects one of the SOMs, which is actually the average of the group and can best represent the rest of the group. It can prevent the effect of outliers and corrupted data on final results.

For HC individuals, the obtained data-driven networks were similar to those found in networks with other clustering methods such as multidimensional clustering [24], info map chart clustering [82], and independent component analysis [59,83] which validates the results of our analysis approach.

Since we used the AAL atlas for network parcellation, our results were the most similar to the results reported in Refs. [59,83]. However, there are some differences in the networks obtained. The data-driven networks of DMN, SMN, VIS, SCN, and FPN were completely consistent with three reference results. In our results, the AUD network was not found by the proposed data-driven approach, which is consistent with the results in Ref. [24]. We assigned cluster number 1, including the posterior cingulate gyrus, hippocampus, parahippocampus, angular

gyrus, thalamus, middle temporal gyrus, and inferior temporal gyrus, to the DMN network according to its anatomical locations and the Hausdorff distance [24,82]. The remaining two clusters were assigned to DAN and VAN networks associated with Yeo and power. The connectivity matrix of these networks demonstrated homogeneity of the obtained networks.

#### 4.1. Abnormal network connectivity in right and left mTLE

Several significant differences in the connectivity of networks between left and right mTLE and HC subjects were observed. In general, participants with mTLE showed a higher within and between-network connectivity compared with the HC cohort. The results of the connectivity change clearly showed that DMN and FPN have been most affected in the within-RSN and between-RSN in terms of increasing the connectivity in LTLE and RTLE, confirming the findings reported in previous studies [19,84–87] that DMN and FPN are affected due to functional defects exhibited by patients with mTLE. This also suggests that mTLE may disrupt brain internal processing and attention networks. Studying the Power and Yeo networks also demonstrated that, DMN, FPN and DAN have been consistently and reliably most affected in the within and between network connectivity across mTLE patients.

DMN plays a crucial role in mTLE. The connectivity alterations between DMN and the other networks could be associated with the structural abnormalities in the hippocampus [10,88,89] as well as ictal and interictal epileptic activities in this area [90] or to episodic memory and/or self-awareness [91,92]. DMN is activated at rest and is thought to be activated when a person focuses on processes of their inner state of mind, such as self-referential processing, biographical memory retrieval, or imagining the future. [92,93]; While DAN and VAN are active in the task mode and are mainly involved in external mental processes for maintenance and re-attention [94]. In addition, FPN is believed to involve in cognitive control functions such as attention, complex problem-solving, working memory, and error monitoring [95]. Also, DMN is a key network because of its ability to integrate information from cognitive networks and key functions [92]. The connection between DMN and task-positive networks (DAN, VAN, and FPN) indicates the existence of an exchange between the internal and external focus of attention in the brain [96,97]. Increased FC between the DMN network and the positive task may lead to network dysfunction and positive and negative tasks in maintaining cognitive function, which may be due to the effect of mTLE on cognitive functions.

The idea that patients with LTLE are more prone to structural changes compared to the patient with RTLE has been mentioned in previous studies [98–101]. Our study and also Power and Yeo networks, show that this pattern also applies to functional activities, including connectivity between cognitive networks, which can be caused by cognitive abnormalities in patients with LTLE and an ineffective attempt to restore these extenuations. In patients with RTLE, only the connection between DMN and FPN was altered using STSOM method, that were a more limited pattern of changes compared to left TLE. Power and Yeo networks were also confirmed by the resulting networks of our proposed method.

In our study, increased connectivity was observed between DMN and VSN in the left TLE cohort. There are studies showing an increase in primary visual cortex activity in mTLE [102,103]. The connectivity alteration between DMN and VIS can be caused by the involvement of the visual network with hippocampal regions [103] altered in mTLE. Therefore, at this point, the hypothesis of the occurrence of increased VIS and DMN connectivity in LTLE as a compensatory mechanism requires further investigation.

Based on our proposed method and also Power and Yeo methods, there were no significant difference between LTLE and RTLE cohorts in FC. Since we used the average of network connectivity for cohorts' comparison, these results show that LTLE and RTLE cohorts are not significantly different in terms of average network connectivity.

However, within and between network connectivity differences between the left mTLE and normal groups, as well as the right mTLE and normal groups, may be useful to the laterality of the left and right mTLE.

#### 4.2. Limitation

Besides reliable findings, our study has some limitations. One major limitation is the relatively small sample size especially for the control and the right mTLE cohorts. Despite we used the reproducibility method for the robustness of our results, increasing the sample size may lead to more reliable and homogeneous results. One of the limitations of this study was the lack of simultaneous EEG recording with this data, thus we cannot analyze and interpret the functional alterations caused by interictal spikes as well as the establishment of the epileptogenic zone as described by previous studies [104].

### 5. Conclusion

In this paper, a new data-driven approach, STSOM, was proposed for clustering the cerebral cortex and the subcortical regions, using brain spatial structure and hemispheric symmetry properties in brain functional networks, without any need for applying binding metrics to the functional connectivity matrix. Calculating the Hausdorff distance between resulted clusters and standard networks, we have demonstrated that the clusters created by our proposed method adequately overlap with the major recognized functional brain networks. In addition to individual-level clustering, we also took a new group-level approach and shared information among individuals. Our results showed that STSOM may identify functional brain networks properly in a wide range of SNR compared to the methods without spatial integration and also simple averaging techniques. Also, proposed method demonstrated to achieve more network homogeneity compared with its null model. Findings for the left and right mTLE patients support a reliable functional interconnection within the functional brain network, and perhaps between them, especially for the default mode and frontoparietal networks, which indicates that there is too frequent information communication between them as a result of epileptic activity and cognitive impairment in patients with mTLE. Besides, increased functional connectivity in negative and task networks may imply major disruption in cognitive networks in mTLE.

#### Ethical approval

All procedures performed in the studies involving human participants were in accordance with the ethical standards of the institutional and/or the national research committee as well as with the 1964 Helsinki declaration and its later amendments or comparable ethical standards.

#### Informed consent

Informed consent was obtained from all individual participants included in the study.

#### Funding

This work was partially funded and supported by Iran's National Elites Foundation, National Institute for Medical Research Development (Grant No. 971683), and Cognitive Sciences & Technologies Council (Grant No. 6431), between 2017 and 2021.

#### Declaration of competing interest

The authors declare that they have no known competing financial interests or personal relationships that could have appeared to influence the work reported in this paper.

## Acknowledgment

The authors recognize the significant contribution of the Iranian National Brain Mapping Laboratory (NBML), Tehran, Iran, for data acquisition services. Also, the authors would like to acknowledge support from Iran Cognitive Sciences & Technologies Council.

## Appendix A. Supplementary data

Supplementary data to this article can be found online at <https://doi.org/10.1016/j.imu.2022.100876>.

## References

- Engel J. Mesial temporal lobe epilepsy: what have we learned? *Neuroscience* 2001;7:340–52. <https://doi.org/10.1177/107385840100700410>.
- Téllez-Zenteno JF, Hernández-Ronquillo L. A review of the epidemiology of temporal lobe epilepsy. *Epilepsy Res Treat* 2012;1–5. <https://doi.org/10.1155/2012/630853>.
- de Campos BM, Coan AC, Lin Yasuda C, Casseb RF, Cendes F. Large-scale brain networks are distinctly affected in right and left mesial temporal lobe epilepsy. *Hum Brain Mapp* 2016;37:3137–52. <https://doi.org/10.1002/hbm.23231>.
- Gross DW, Concha L, Beaulieu C. Extratemporal white matter abnormalities in mesial temporal lobe epilepsy demonstrated with diffusion tensor imaging. *Epilepsia* 2006;47:1360–3. <https://doi.org/10.1111/j.1528-1167.2006.00603.x>.
- Keller SS, Roberts N. Voxel-based morphometry of temporal lobe epilepsy: an introduction and review of the literature. *Epilepsia* 2008;49:741–57. <https://doi.org/10.1111/j.1528-1167.2007.01485.x>.
- Bonilha L. Medial temporal lobe atrophy in patients with refractory temporal lobe epilepsy. *J Neurol Neurosurg Psychiatry* 2003;74:1627–30. <https://doi.org/10.1136/jnnp.74.12.1627>.
- Keller SS. Voxel based morphometry of grey matter abnormalities in patients with medically intractable temporal lobe epilepsy: effects of side of seizure onset and epilepsy duration. *J Neurol Neurosurg Psychiatry* 2002;73:648–55. <https://doi.org/10.1136/jnnp.73.6.648>.
- Bonilha L, Rorden C, Castellano G, Cendes F, Li LM. Voxel-based morphometry of the thalamus in patients with refractory medial temporal lobe epilepsy. *Neuroimage* 2005;25:1016–21. <https://doi.org/10.1016/j.neuroimage.2004.11.050>.
- Mahmoudi F, Elisevich K, Bagher-Ebadian H, Nazem-Zadeh MR, Davoodi-Bojd E, Schwalb JM, Kaur M, Soltanian-Zadeh H. Data mining MR image features of select structures for lateralization of mesial temporal lobe epilepsy. *PLoS One* 2018;13:1–19. <https://doi.org/10.1371/journal.pone.0199137>.
- Nazem-Zadeh M-R, Schwalb JM, Elisevich KV, Bagher-Ebadian H, Hamidian H, Akhondi-Asl A-R, Jafari-Khouzani K, Soltanian-Zadeh H. Lateralization of temporal lobe epilepsy using a novel uncertainty analysis of MR diffusion in hippocampus, cingulum, and fornix, and hippocampal volume and FLAIR intensity. *J Neurol Sci* 2014;342:152–61. <https://doi.org/10.1016/j.jns.2014.05.019>.
- Fallahi A, Pooyan M, Habibabadi JM, Nazem-Zadeh MR. Comparison of multimodal findings on epileptogenic side in temporal lobe epilepsy using self-organizing maps. *Magn Reson Mater Physics, Biol Med* 2021. <https://doi.org/10.1007/s10334-021-00948-7>.
- Salmond CH, Ashburner J, Vargha-Khadem F, Connelly A, Gadian DG, Friston KJ. Distributional assumptions in voxel-based morphometry. *Neuroimage* 2002;17:1027–30.
- Bonilha L, Rorden C, Halford JJ, Eckert M, Appenzeller S, Cendes F, Li LM. Asymmetrical extra-hippocampal grey matter loss related to hippocampal atrophy in patients with medial temporal lobe epilepsy. *J Neurol Neurosurg Psychiatry* 2006;78:286–94. <https://doi.org/10.1136/jnnp.2006.103994>.
- Pereira FR, Alessio A, Sercheli MS, Pedro T, Bilevicius E, Rondina JM, Ozelo HF, Castellano G, Covolan RJ, Damasceno BP, Cendes F. Asymmetrical hippocampal connectivity in mesial temporal lobe epilepsy: evidence from resting state fMRI. *BMC Neurosci* 2010;11:66. <https://doi.org/10.1186/1471-2202-11-66>.
- Jamali-Dinan S-S, Soltanian-Zadeh H, Bowyer SM, Almohri H, Dehghani H, Elisevich K, Nazem-Zadeh M-R. A combination of particle swarm optimization and Minkowski weighted K-means clustering: application in lateralization of temporal lobe epilepsy. *Brain Topogr* 2020;33:519–32. <https://doi.org/10.1007/s10548-020-00770-9>.
- Engel Jr J, Thompson PM, Stern JM, Staba RJ, Bragin A, Mody I. Connectomics and epilepsy. *Curr Opin Neurol* 2013;26:186–94. <https://doi.org/10.1097/WCO.0b013e32835ee5b8>.
- Chiang S, Stern JM, Engel J, Levin HS, Haneef Z. Differences in graph theory functional connectivity in left and right temporal lobe epilepsy. *Epilepsy Res* 2014;108:1770. <https://doi.org/10.1016/j.epilepsyres.2014.09.023>. –1781.
- Stretton J, Thompson PJ. Frontal lobe function in temporal lobe epilepsy. *Epilepsy Res* 2012;98:1–13. <https://doi.org/10.1016/j.epilepsyres.2011.10.009>.
- Haneef Z, Lenartowicz A, Yeh HJ, Engel J, Stern JM. Effect of lateralized temporal lobe epilepsy on the default mode network. *Epilepsy Behav* 2012;25:350–7. <https://doi.org/10.1016/j.yebeh.2012.07.019>.
- Su L, An J, Ma Q, Qiu S, Hu D. Influence of resting-state network on lateralization of functional connectivity in mesial temporal lobe epilepsy. *Am J Neuroradiol* 2015;36:1479–87. <https://doi.org/10.3174/ajnr.A4346>.
- Fallahi A, Pooyan M, Lotfi N, Baniasad F, Tapak L, Mohammadi-Mobarakeh N, Hashemi-Fesharaki SS, Mehvari-Habibabadi J, Ay MR, Nazem-Zadeh M-R. Dynamic functional connectivity in temporal lobe epilepsy: a graph theoretical and machine learning approach. *Neurol Sci* 2020. <https://doi.org/10.1007/s10072-020-04759-x>.
- Biswal B, Zerrin Yetkin F, Haughton VM, Hyde JS. Functional connectivity in the motor cortex of resting human brain using echo-planar MRI. *Magn Reson Med* 1995;34:537–41. <https://doi.org/10.1002/mrm.1910340409>.
- Power JD, Cohen AL, Nelson SM, Wig GS, Barnes KA, Church JA, Vogel AC, Laumann TO, Miezin FM, Schlaggar BL, Petersen SE. Functional network organization of the human brain. *Neuron* 2011;72:665–78. <https://doi.org/10.1016/j.neuron.2011.09.006>.
- Thomas Yeo BT, Krienen FM, Sepulcre J, Sabuncu MR, Lashkari D, Hollinshead M, Roffman JL, Smoller JW, Zöllei L, Polimeni JR, Fisch B, Liu H, Buckner RL. The organization of the human cerebral cortex estimated by intrinsic functional connectivity. *J Neurophysiol* 2011;106:1125–65. <https://doi.org/10.1152/jn.00338.2011>.
- Schaefer A, Kong R, Gordon EM, Laumann TO, Zuo X-N, Holmes AJ, Eickhoff SB, Yeo BT. Local-global parcellation of the human cerebral cortex from intrinsic functional connectivity MRI. *Cerebr Cortex* 2018;28:3095–114. <https://doi.org/10.1093/cercor/bhx179>.
- Craddock RC, James GA, Holtzheimer PE, Hu XP, Mayberg HS. A whole brain fMRI atlas generated via spatially constrained spectral clustering. *Hum Brain Mapp* 2012;33:1914–28. <https://doi.org/10.1002/hbm.21333>.
- Shen X, Tokoglu F, Papademetris X, Constable RT. Groupwise whole-brain parcellation from resting-state fMRI data for network node identification. *Neuroimage* 2013;82:403–15. <https://doi.org/10.1016/j.neuroimage.2013.05.081>.
- Fischl B, Rajendran N, Busa E, Augustinack J, Hinds O, Yeo BT, Mohlberg H, Amunts K, Zilles K. Cortical folding patterns and predicting cytoarchitecture. *Cerebr Cortex* 2008;18:1973. <https://doi.org/10.1093/cercor/bhm225>. –1980.
- Raemaekers M, Schellekens W, Petridou N, Ramsey NF. Knowing left from right: asymmetric functional connectivity during resting state. *Brain Struct Funct* 2018. <https://doi.org/10.1007/s00429-017-1604-y>.
- Damoiseaux JS, Rombouts SAR, Barkhof F, Scheltens P, Stam CJ, Smith SM, Beckmann CF. Consistent resting-state networks across healthy subjects. *Proc Natl Acad Sci Unit States Am* 2006;103:13848–53. <https://doi.org/10.1073/pnas.0601417103>.
- Smith SM, Fox PT, Miller KL, Glahn DC, Fox PM, Mackay CE, Filippini N, Watkins KE, Toro R, Laird AR, Beckmann CF. Correspondence of the brain's functional architecture during activation and rest. *Proc Natl Acad Sci U S A* 2009;106:13040–5. <https://doi.org/10.1073/pnas.05267106>.
- Ma Sai, Correa NM, Li Xi-Lin, Eichele T, Calhoun VD, Adali T. Automatic identification of functional clusters in fMRI data using spatial dependence. *IEEE Trans Biomed Eng* 2011;58:3406–17. <https://doi.org/10.1109/TBME.2011.2167149>.
- Liao Wei, Chen Huafu, Yang Qin, Xu Lei. Analysis of fMRI data using improved self-organizing mapping and spatio-temporal metric hierarchical clustering. *IEEE Trans Med Imag* 2008;27:1472–83. <https://doi.org/10.1109/TMI.2008.923987>.
- Hansen LK, Larsen J, Nielsen FÅ, Strother SC, Rostrup E, Savoy R, Lange N, Sidtis J, Svarer C, Paulson OB. Generalizable patterns in neuroimaging: how many principal components? *Neuroimage* 1999;9:534–44. <https://doi.org/10.1006/nimg.1998.0425>.
- Leonardi N, Richiardi J, Gschwind M, Simioni S, Annoni JM, Schluep M, Vuilleumier P, Van De Ville D. Principal components of functional connectivity: a new approach to study dynamic brain connectivity during rest. *Neuroimage* 2013;83:937–50. <https://doi.org/10.1016/j.neuroimage.2013.07.019>.
- Calhoun VD, Adali T, Pearlson GD, Pekar JJ. Spatial and temporal independent component analysis of functional MRI data containing a pair of task-related waveforms. *Hum Brain Mapp* 2001;13:43–53. <https://doi.org/10.1002/hbm.1024>.
- Schöpf V, Windischberger C, Kassess CH, Lanzenberger R, Moser E. Group ICA of resting-state data: a comparison. *Magn Reson Mater Physics, Biol Med* 2010;23:317–25. <https://doi.org/10.1007/s10334-010-0212-0>.
- Goutte C, Toft P, Rostrup E, Nielsen FÅ, Hansen LK. On clustering fMRI time series. *Neuroimage* 1999;9:298–310. <https://doi.org/10.1006/nimg.1998.0391>.
- Katwal SB, Gore JC, Marois R, Rogers BP. Unsupervised spatiotemporal analysis of fMRI data using graph-based visualizations of self-organizing maps. *IEEE Trans Biomed Eng* 2013;60:2472–83. <https://doi.org/10.1109/TBME.2013.2258344>.
- Cordes D, Haughton V, Carew JD, Arfanakis K, Maravilla K. Hierarchical clustering to measure connectivity in fMRI resting-state data. *Magn Reson Imaging* 2002;20:305–17. [https://doi.org/10.1016/S0730-725X\(02\)00503-9](https://doi.org/10.1016/S0730-725X(02)00503-9).
- Wismüller A, Meyer-Bäse A, Lange O, Auer D, Reiser MF, Summers D. Model-free functional MRI analysis based on unsupervised clustering. *J Biomed Inf* 2004;37:10–8. <https://doi.org/10.1016/j.jbi.2003.12.002>.
- Peltier SJ, Polk TA, Noll DC. Detecting low-frequency functional connectivity in fMRI using a self-organizing map (SOM) algorithm. <https://doi.org/10.1002/hbm.10144>; 2003. 226:220–226.
- Liao W, Chen H, Yang Q, Lei X. Analysis of fMRI data using improved self-organizing mapping and spatio-temporal metric hierarchical clustering. *IEEE Trans Med Imag* 2008;27:1472–83. <https://doi.org/10.1109/TMI.2008.923987>.

- [44] Jia Y, Gu H. Sample entropy combined with the K-means clustering algorithm reveals six functional networks of the brain. *Entropy* 2019;21:1–18. <https://doi.org/10.3390/e21121156>.
- [45] Le TH, Hu X. Potential pitfalls of principal component analysis in fMRI. *Magnetic resonance in medicine*, 3rd annual meeting, vol. 820; 1995.
- [46] Mckeown MJ, Makeig S, Brown GG, Jung T-P, Kindermann SS, Bell AJ, Sejnowski TJ. Analysis of fMRI data by blind separation into independent spatial components. *Hum Brain Mapp* 1998;6:160–88. [https://doi.org/10.1002/\(SICI\)1097-0193\(1998\)6:3<160::AID-HBM5>3.0.CO;2-1](https://doi.org/10.1002/(SICI)1097-0193(1998)6:3<160::AID-HBM5>3.0.CO;2-1).
- [47] Daubechies I, Roussos E, Takerkart S, Benharrosh M, Golden C, D'Ardenne K, Richter W, Cohen JD, Haxby J. Independent component analysis for brain fMRI does not select for independence. *Proc Natl Acad Sci Unit States Am* 2009;106:10415–22. <https://doi.org/10.1073/pnas.0903525106>.
- [48] Chuang Kai-Hsiang, Chiu Ming-Jang, Lin Chung-Chih, Chen Jyh-Hong. Model-free functional MRI analysis using Kohonen clustering neural network and fuzzy C-means. *IEEE Trans Med Imag* 1999;18:1117–28. <https://doi.org/10.1109/42.819322>.
- [49] Kohonen T. The self-organizing map. *Neurocomputing* 1998;21:1–6. [https://doi.org/10.1016/S0925-2312\(98\)00030-7](https://doi.org/10.1016/S0925-2312(98)00030-7).
- [50] Kohonen T. Essentials of the self-organizing map. *Neural Network* 2013;37:52–65. <https://doi.org/10.1016/j.neunet.2012.09.018>.
- [51] Fournel AP, Reynaud E, Brammer MJ, Simmons A, Ginetet CE. Group analysis of self-organizing maps based on functional MRI using restricted Frechet means. *Neuroimage* 2013;76:373–85. <https://doi.org/10.1016/j.neuroimage.2013.02.043>.
- [52] Yan C-G, Wang X-D, Zuo X-N, Zang Y-F. DPABI: data processing & analysis for (Resting-State) brain imaging. *Neuroinformatics* 2016;14:339–51. <https://doi.org/10.1007/s12021-016-9299-4>.
- [53] Tzourio-Mazoyer N, Landeau B, Papathanassiou D, Crivello F, Etard O, Delcroix N, Mazoyer B, Joliot M. Automated anatomical labeling of activations in SPM using a macroscopic anatomical parcellation of the MNI MRI single-subject brain. *Neuroimage* 2002;15:273–89. <https://doi.org/10.1006/nimg.2001.0978>.
- [54] Power JD, Barnes KA, Snyder AZ, Schlaggar BL, Petersen SE. Spurious but systematic correlations in functional connectivity MRI networks arise from subject motion. *Neuroimage* 2012;59:2142–54. <https://doi.org/10.1016/j.neuroimage.2011.10.018>.
- [55] Erhardt EB, Allen EA, Wei Y, Eichele T, Calhoun VD, SimTB, a simulation toolbox for fMRI data under a model of spatiotemporal separability. *Neuroimage* 2012;59:4160–7. <https://doi.org/10.1016/j.neuroimage.2011.11.088>.
- [56] Allen EA, Damaraju E, Plis SM, Erhardt EB, Eichele T, Calhoun VD. Tracking whole-brain connectivity dynamics in the resting state. *Cerebr Cortex* 2014;24:663–76. <https://doi.org/10.1093/cercor/bhs352>.
- [57] Ting C-M, Ombao H, Samdin SB, Salleh S-H. Estimating dynamic connectivity states in fMRI using regime-switching factor models. *IEEE Trans Med Imag* 2018;37:1011–23. <https://doi.org/10.1109/TMI.2017.2780185>.
- [58] Fisher RA. Frequency distribution of the values of the correlation coefficient in samples from an indefinitely large population. *Biometrika* 1915;10:507. <https://doi.org/10.2307/2331838>.
- [59] Allen EA, Damaraju E, Plis SM, Erhardt EB, Eichele T, Calhoun VD. Tracking whole-brain connectivity dynamics in the resting state. *Cerebr Cortex* 2014;24:663–76. <https://doi.org/10.1093/cercor/bhs352>.
- [60] Vesanto J, Alhoniemi E. Clustering of the self-organizing map. *IEEE Trans Neural Network* 2000;11:586–600. <https://doi.org/10.1109/72.846731>.
- [61] Park Y-S, Céréghino R, Compain A, Lek S. Applications of artificial neural networks for patterning and predicting aquatic insect species richness in running waters. *Ecol Model* 2003;160:265–80. [https://doi.org/10.1016/S0304-3800\(02\)00258-2](https://doi.org/10.1016/S0304-3800(02)00258-2).
- [62] Ki SJ, Kang J-H, Lee SW, Lee YS, Cho KH, An K-G, Kim JH. Advancing assessment and design of stormwater monitoring programs using a self-organizing map: characterization of trace metal concentration profiles in stormwater runoff. *Water Res* 2011;45:4183–97. <https://doi.org/10.1016/j.watres.2011.05.021>.
- [63] Tobiszewski M, Tsakovski S, Simeonov V, Namieśnik J. Chlorinated solvents in a petrochemical wastewater treatment plant: an assessment of their removal using self-organising maps. *Chemosphere* 2012;87:962–8. <https://doi.org/10.1016/j.chemosphere.2012.01.057>.
- [64] Davies DL, Bouldin DW. A cluster separation measure. *IEEE Trans Pattern Anal Mach Intell PAMI-* 1979;1:224–7. <https://doi.org/10.1109/TPAMI.1979.4766909>.
- [65] Rousseeuw PJ. Silhouettes: a graphical aid to the interpretation and validation of cluster analysis. *J Comput Appl Math* 1987;20:53–65. [https://doi.org/10.1016/0377-0427\(87\)90125-7](https://doi.org/10.1016/0377-0427(87)90125-7).
- [66] Thorndike RL. Who belongs in the family? *Psychometrika* 1953;18:267–76. <https://doi.org/10.1007/BF02289263>.
- [67] Çinar Ö, Merdun H. Application of an unsupervised artificial neural network technique to multivariate surface water quality data. *Ecol Res* 2009;24:163–73. <https://doi.org/10.1007/s11284-008-0495-z>.
- [68] Nguyen TT, Kawamura A, Tong TN, Nakagawa N, Amaguchi H, Gilbuena R. Clustering spatio-seasonal hydrogeochemical data using self-organizing maps for groundwater quality assessment in the Red River Delta, Vietnam. *J Hydrol* 2015;522:661–73. <https://doi.org/10.1016/j.jhydrol.2015.01.023>.
- [69] Li T, Sun G, Yang C, Liang K, Ma S, Huang L. Science of the Total Environment Using self-organizing map for coastal water quality classification: towards a better understanding of patterns and processes. *Sci Total Environ* 2018;628–629:1446–59. <https://doi.org/10.1016/j.scitotenv.2018.02.163>.
- [70] Wang Y-B, Liu C-W, Wang S-W. Characterization of heavy-metal-contaminated sediment by using unsupervised multivariate techniques and health risk assessment. *Ecotoxicol Environ Saf* 2015;113:469–76. <https://doi.org/10.1016/j.ecoenv.2014.12.036>.
- [71] Deng D. Content-based image collection summarization and comparison using self-organizing maps. *Pattern Recogn* 2007;40:718–27. <https://doi.org/10.1016/j.patcog.2006.05.022>.
- [72] Gordon EM, Laumann TO, Adeyemo B, Huckins JF, Kelley WM, Petersen SE. Generation and evaluation of a cortical area parcellation from resting-state correlations. *Cerebr Cortex* 2016;26:288–303. <https://doi.org/10.1093/cercor/bhu239>.
- [73] Meyer-Baese A, Wismueller A, Lange O. Comparison of two exploratory data analysis methods for fMRI: unsupervised clustering versus independent component analysis. *IEEE Trans Inf Technol Biomed* 2004;8:387–98. <https://doi.org/10.1109/TITB.2004.834406>.
- [74] Wang D, Buckner RL, Liu H. Functional specialization in the human brain estimated by intrinsic hemispheric interaction. *J Neurosci* 2014;34:12341–52. <https://doi.org/10.1523/JNEUROSCI.0787-14.2014>.
- [75] Joliot M, Tzourio-Mazoyer N, Mazoyer B. Intra-hemispheric intrinsic connectivity asymmetry and its relationships with handedness and language Lateralization. *Neuropsychologia* 2016;93:437–47. <https://doi.org/10.1016/j.neuropsychologia.2016.03.013>.
- [76] Muller AM, Meyer M. Language in the brain at rest: new insights from resting state data and graph theoretical analysis. *Front Hum Neurosci* 2014;8. <https://doi.org/10.3389/fnhum.2014.00228>.
- [77] Branco P, Seixas D, Castro SL. Mapping language with resting-state functional magnetic resonance imaging: a study on the functional profile of the language network. *Hum Brain Mapp* 2020;41:545–60. <https://doi.org/10.1002/hbm.24821>.
- [78] Tanaka N, Stufflebeam SM. Presurgical mapping of the language network using resting-state functional connectivity. *Top Magn Reson Imag* 2016;25:19–24. <https://doi.org/10.1097/RMR.000000000000073>.
- [79] van den Heuvel M, Mandl R, Pol HH. Normalized cut group clustering of resting-state fMRI data. *PLoS One* 2008;3. <https://doi.org/10.1371/journal.pone.0002001>.
- [80] Glerean E, Pan RK, Salmi J, Kujala R, Lahnakoski JM, Roine U, Nummenmaa L, Leppämäki S, Nieminen-von Wendt T, Tani P, Saramäki J, Sams M, Jääskeläinen IP. Reorganization of functionally connected brain subnetworks in high-functioning autism. *Hum Brain Mapp* 2016;37:1066–79. <https://doi.org/10.1002/hbm.23084>.
- [81] Gordon EM, Laumann TO, Adeyemo B, Gilmore AW, Nelson SM, Dosenbach NUF, Petersen SE. Individual-specific features of brain systems identified with resting state functional correlations. *Neuroimage* 2017;146:918–39. <https://doi.org/10.1016/j.neuroimage.2016.08.032>.
- [82] Power JD, Cohen AL, Nelson SM, Wig GS, Barnes KA, Church JA, Vogel AC, Laumann TO, Miezin FM, Schlaggar BL, Petersen SE. Functional network organization of the human brain. *Neuron* 2011;72:665–78. <https://doi.org/10.1016/j.neuron.2011.09.006>.
- [83] Li R, Chen K, Fleisher AS, Reiman EM, Yao L, Wu X. Large-scale directional connections among multi resting-state neural networks in human brain: a functional MRI and Bayesian network modeling study. *Neuroimage* 2011;56:1035–42. <https://doi.org/10.1016/j.neuroimage.2011.03.010>.
- [84] Liao W, Zhang Z, Pan Z, Mantini D, Ding J, Duan X, Luo C, Lu G, Chen H. Altered functional connectivity and small-world in mesial temporal lobe epilepsy. *PLoS One* 2010;5:27–9. <https://doi.org/10.1371/journal.pone.0008525>.
- [85] Liao W, Zhang Z, Pan Z, Mantini D, Ding J, Duan X, Luo C, Wang Z, Tan Q, Lu G, Chen H. Default mode network abnormalities in mesial temporal lobe epilepsy: a study combining fMRI and DTI. *Hum Brain Mapp* 2011;32:883–95. <https://doi.org/10.1002/hbm.21076>.
- [86] Zhang C, Yang H, Liu C, Zhang G, Chen N, Li K. Brain network alterations of mesial temporal lobe epilepsy with cognitive dysfunction following anterior temporal lobectomy. *Epilepsy Behav* 2018;87:123–30. <https://doi.org/10.1016/j.yebeh.2018.07.021>.
- [87] Jia X, Xie Y, Dong D, Pei H, Jiang S, Ma S, Huang Y, Zhang X, Wang Y, Zhu Q, Zhang Y, Yao D, Yu L, Luo C. Reconfiguration of dynamic large-scale brain network functional connectivity in generalized tonic-clonic seizures. *Hum Brain Mapp* 2020;41:67–79. <https://doi.org/10.1002/hbm.24787>.
- [88] Nazem-Zadeh MR, Elisevich KV, Schwalb JM, Bagher-Ebadian H, Mahmoudi F, Soltanian-Zadeh H. Lateralization of temporal lobe epilepsy by multimodal multinomial hippocampal response-driven models. *J Neurol Sci* 2014;347:107–18. <https://doi.org/10.1016/j.jns.2014.09.029>.
- [89] Sanjari Moghaddam H, Rahmani F, Aarabi MH, Nazem-Zadeh MR, Davoodi-Bojd E, Soltanian-Zadeh H. White matter microstructural differences between right and left mesial temporal lobe epilepsy. *Acta Neurol Belg* 2019. <https://doi.org/10.1007/s13760-019-01074-x>. 0:0.
- [90] Zhang Z, Lu G, Zhong Y, Tan Q, Liao W, Wang Z, Wang Z, Li K, Chen H, Liu Y. Altered spontaneous neuronal activity of the default-mode network in mesial temporal lobe epilepsy. *Brain Res* 2010;1323:152–60. <https://doi.org/10.1016/j.brainres.2010.01.042>.
- [91] Yang T, Luo C, Li Q, Guo Z, Liu L, Gong Q, Yao D, Zhou D. Altered resting-state connectivity during interictal generalized spike-wave discharges in drug-naïve childhood absence epilepsy. *Hum Brain Mapp* 2013;34:1761–7. <https://doi.org/10.1002/hbm.22025>.
- [92] Raichle ME, MacLeod AM, Snyder AZ, Powers WJ, Gusnard DA, Shulman GL. A default mode of brain function. *Proc Natl Acad Sci Unit States Am* 2001;98:676–82. <https://doi.org/10.1073/pnas.98.2.676>.
- [93] Brewer JA, Worhunsky PD, Gray JR, Tang Y-Y, Weber J, Kober H. Meditation experience is associated with differences in default mode network activity and

- connectivity. *Proc Natl Acad Sci Unit States Am* 2011;108:20254–9. <https://doi.org/10.1073/pnas.1112029108>.
- [94] Christoff K, Irving ZC, Fox KCR, Spreng RN, Andrews-Hanna JR. Mind-wandering as spontaneous thought: a dynamic framework. *Nat Rev Neurosci* 2016;17:718–31. <https://doi.org/10.1038/nrn.2016.113>.
- [95] Vincent JL, Kahn I, Snyder AZ, Raichle ME, Buckner RL. Evidence for a frontoparietal control system revealed by intrinsic functional connectivity. *J Neurophysiol* 2008;100:3328–42. <https://doi.org/10.1152/jn.90355.2008>.
- [96] Weissman DH, Roberts KC, Visscher KM, Woldorff MG. The neural bases of momentary lapses in attention. *Nat Neurosci* 2006;9:971–8. <https://doi.org/10.1038/nn1727>.
- [97] Whitfield-Gabrieli S, Ford JM. Default mode network activity and connectivity in psychopathology. *Annu Rev Clin Psychol* 2012;8:49–76. <https://doi.org/10.1146/annurev-clinpsy-032511-143049>.
- [98] Nazem-Zadeh MR, Elisevich K, Air EL, Schwalb JM, Divine G, Kaur M, Wasade VS, Mahmoudi F, Shokri S, Bagher-Ebadian H, Soltanian-Zadeh H. DTI-based response-driven modeling of mTLE laterality. *NeuroImage Clin* 2016;11:694–706. <https://doi.org/10.1016/j.nicl.2015.10.015>.
- [99] Nazem-Zadeh M-R, Bowyer SM, Moran JE, Davoodi-Bojd E, Zillgitt A, Weiland BJ, Bagher-Ebadian H, Mahmoudi F, Elisevich K, Soltanian-Zadeh H. MEG coherence and DTI connectivity in mTLE. *Brain Topogr* 2016;29:598–622. <https://doi.org/10.1007/s10548-016-0488-0>.
- [100] Ahmadi ME, Hagler DJ, McDonald CR, Tecoma ES, Iragui VJ, Dale AM, Halgren E. Side matters: diffusion tensor imaging tractography in left and right temporal lobe epilepsy. *Am J Neuroradiol* 2009;30:1740–7. <https://doi.org/10.3174/ajnr.A1650>.
- [101] Coan AC, Appenzeller S, Bonilha L, Li LM, Cendes F. Seizure frequency and lateralization affect progression of atrophy in temporal lobe epilepsy. *Neurology* 2009;73:834–42. <https://doi.org/10.1212/WNL.0b013e3181b783dd>.
- [102] Zhang Z, Lu G, Zhong Y, Tan Q, Liao W, Chen Z, Shi J, Liu Y. Impaired perceptual networks in temporal lobe epilepsy revealed by resting fMRI. *J Neurol* 2009;256:1705–13. <https://doi.org/10.1007/s00415-009-5187-2>.
- [103] Lee K, Khoo HM, Lina JM, Dubeau F, Gotman J, Grova C. Disruption, emergence and lateralization of brain network hubs in mesial temporal lobe epilepsy. *NeuroImage Clin* 2018;20:71–84. <https://doi.org/10.1016/j.nicl.2018.06.029>.
- [104] Coan AC, Campos BM, Beltramini GC, Yasuda CL, Covolan RJM, Cendes F. Distinct functional and structural MRI abnormalities in mesial temporal lobe epilepsy with and without hippocampal sclerosis. *Epilepsia* 2014;55:1187–96. <https://doi.org/10.1111/epi.12670>.